Cyclin-dependent kinase 1-mediated AMPK phosphorylation regulates chromosome alignment and mitotic progression

Seth Stauffer[a,b], Yongji Zeng[a,b], Montserrat Santos[c], Jiuli Zhou[a,b], Yuanhong Chen[a] and Jixin Dong[a,1]

[a]Eppley Institute for Research in Cancer & Allied Diseases, Fred & Pamela Buffett Cancer Center

[b]Department of Pathology and Microbiology,

University of Nebraska Medical Center, Omaha, NE 68198.

[c]Department of Chemistry and Department of Biology, College of Saint Mary, Omaha, NE 68106.

[1] To whom correspondence should be addressed:

Eppley Institute for Research in Cancer & Allied Diseases

University of Nebraska Medical Center

986805 Nebraska Medical Center, Omaha, NE 68198-6805.

Phone: 402-559-5596

Fax: 402-559-4651

Email: dongj@unmc.edu

JCS Advance Online Article. Posted on 13 September 2019

ABSTRACT

AMP-activated protein kinase (AMPK), a heterotrimeric serine/threonine kinase and cellular metabolic sensor, has been found to regulate cell cycle checkpoints in cancer cells in response to energetic stress to harmonize proliferation with energy availability. Despite AMPK's emergent association with the cell cycle, it still has not been fully delineated how AMPK is regulated by upstream signaling pathways during mitosis. We report, for the first time, direct CDK1 phosphorylation of both the catalytic α1 and α2 subunits as well as the β1 regulatory subunit of AMPK in mitosis. We found that AMPK-knockout U2OS osteosarcoma cells have reduced mitotic indexes and that CDK1 phosphorylation-null AMPK is unable to rescue the phenotype, demonstrating a role for CDK1 regulation of mitotic entry through AMPK. Our results also denote a vital role for AMPK in promoting proper chromosomal alignment, as loss of AMPK activity leads to misaligned chromosomes and concomitant metaphase delay. Importantly, AMPK expression and activity was found to be critical for paclitaxel chemosensitivity in breast cancer cells and positively correlated with relapse-free survival in systemically treated breast cancer patients.

Key words: AMPK; Mitotic phosphorylation; CDK1; Taxol sensitivity

INTRODUCTION

Mitosis is a dynamic and vitally important process for separating identical copies of genomic material into two daughter cells. It is thought that failure in the mitotic processes can lead to tumor initiation [1-3]. One of the hallmarks of cancer is mitotic defects, frequently seen as flaws in chromosomal adhesion, spindle attachment, chromosomal segregation, cytokinesis, and centrosomal duplication [4-6]. Another important path to cellular transformation is a change in the fidelity of mitotic checkpoints. Mutations or aberrations in the regulation of cell cycle checkpoints often result in what is known as mitotic cell death (MCD) [7] or lead to cancer [8, 9], indicating the importance of these checkpoints.

Dramatic changes to major organelles and cellular organization happen swiftly during this relatively short period of the cell cycle. This window is considered the most vulnerable period of the cell cycle and, subsequently, has become the target of multiple anti-cancer drugs. Many aim to activate the spindle assembly checkpoint (SAC) or to target components of the anaphase-promoting complex (APC), leading to prolonged mitotic arrest, and eventual activation of pathways promoting MCD [10]. Thus, identifying additional molecular regulation in mitosis may lead to the identification of potentially druggable targets and development of novel chemotherapeutics for combatting cancer.

AMPK is a heterotrimeric serine/threonine kinase consisting of a catalytic α subunit and two regulatory β and γ subunits. Known to be phosphorylated by kinases LKB1 and CAMKK, AMPK regulates cellular energy homeostasis and harmonizes proliferation with energy availability. Additionally, proliferation is adjusted through metabolic signals which have been shown previously to be coupled to cell cycle progression [11]. Of importance, AMPK has been found to sit in the center of a signaling network involving bona fide tumor suppressors [12] and found to be associated with cell cycle checkpoints, as AMPK-null *Drosophila* cells have mitotic defects [13]. AMPK has also been found to be activated during mitosis with increased p-T172 phosphorylation

seen during mitosis [14-19]. Likewise, a screen of AMPK substrates revealed multiple downstream mitotic proteins as targets of its kinase activity [20]. A chemical genetic screen of downstream AMPK substrates in human cells identified several which were involved in mitosis including protein phosphatase 1 regulatory subunit 12A and 12C (PPP1R12A/2C), cell division cycle protein 27 (CDC27), and p21-activated protein kinase (PAK2) [20]. AMPK phosphorylation of PPP1R12C blocks its inhibition of myosin regulatory light chain (MRLC) which is a regulator of cytokinesis [21], CDC27 is a member of the APC connecting AMPK to the spindle checkpoint during metaphase [22], and AMPK activation of PAK2 leads to phosphorylation of MRLC and mitotic progression [23]. MRLC has also been shown to be phosphorylated directly by AMPK at its regulatory site *in vitro* and *in vivo*, both in *Drosophila* and mammals [24]. AMPK has been connected to mitosis in other studies as well. AMPK-null *Drosophila* embryos display severe abnormalities in cytoskeletal apical-basal polarity as well as defective mitotic divisions which lead to polyploidy [13]. Loss of AMPK activity, through either inhibition of AMPK in cancer cells [25] or with full AMPK knockout (KO) in mouse embryonic fibroblasts (MEFs) [26], is enough to weaken the cell cycle arrest at G_2/M caused by ionizing radiation. Interestingly, due to the important role microtubules play in mitotic cell division, inhibition of AMPK has been shown to impair microtubule stabilization through loss of phosphoregulation of the microtubule plus-end protein CLIP-170 [27]. There is evidence that CLIP-170, itself, mediates paclitaxel sensitivity in breast cancer cells through its ability to strengthen microtubule assembly promoted by paclitaxel [28]. AMPK is also active in the mitotic regulation of neural stem cells. Abolishing normal AMPK activity in the developing mouse brain leads to flawed mitosis in neural progenitor cells and abnormal brain development [29]. Recently, it has been discovered that AMPK and its ortholog Snf1 in *S. cerevisiae* are required for proper metaphase spindle alignment [15, 30]. Together, these studies point to a role for AMPK outside of its canonical signaling network, acting as a master regulator not only of cellular metabolism, but also cell cycle progression. Despite AMPK's connection to

mitosis, how AMPK is regulated during mitotic progression remains unclear. In this report, we identify a novel layer of regulation involving CDK1-mediated phosphorylation for AMPK.

RESULTS

AMPK is phosphorylated during antitubulin drug-induced mitotic arrest

To examine the phosphorylation status of the AMPK subunits, we used PhosTag gel electrophoresis which selectively separates phosphorylated from unphosphorylated proteins through specific binding of phosphate ions (see [31, 32]). The mobility shifts of AMPKα1, α2, and β1 were seen to be increased during mitotic arrest induced by antimitotic drugs (Fig. 1A), suggesting that AMPK is phosphorylated during mitotic arrest. The mobility of AMPKβ2, AMPKγ1, AMPKγ2 and AMPKγ3 were not altered under these conditions (Fig. 1A). We found that the phosphorylation levels of AMPKα1/α2 at the main T172 activation site and AMPKβ1 at S108 and S182 were not changed under these conditions. This suggests that the mobility shift of AMPK was not likely due to phosphorylation at T172 or S108/S182 respectively and indicates the possibility of novel post-translational modification sites (Fig. 1B). Treatment of arrested cells with λ-phosphatase completely reversed the mobility shift of AMPKα and β1 (Fig. 1C), indicating that the mobility shifts of AMPK subunits during mitosis were due to phosphorylation events. In order to determine which upstream kinases could be phosphorylating AMPK, we took cells that were cultured overnight with taxol and then treated for two hours with various kinase inhibitors. Interestingly, only the CDK1 inhibitors RO-3306 and Purvalanol A were able to block the mobility shift for AMPKα (Fig. 1D) and β1 (Fig. 1E), signifying that possibly CDK1 is phosphorylating AMPK directly or may be acting further upstream. Taken together, these data suggest that mitotic arrest-induced AMPK phosphorylation is CDK1 dependent.

CDK1 phosphorylates AMPK in vitro

In vitro kinase assays were performed to determine whether CDK1 can directly phosphorylate AMPKα, with GST-tagged AMPKα as substrate. Lysates of taxol-treated mitotic cells strongly phosphorylated AMPKα, and RO-3306 inhibition of CDK1 significantly reduced phosphorylation of GST-AMPKα (Fig. 2A). Database analysis revealed multiple sites in AMPK α1, α2, and β1 as mitotic phosphorylation sites from large-scale phosphoproteomic studies [33-35]. Scanning the amino acid sequences of the AMPK α1 and α2 subunits for CDK1 consensus motifs identified two potential phosphorylated sites: T382 and T490 on α1 and S377 and T485 on α2 which are located in the AMPKα ST-stretch (Fig. 2B). Cross-species alignment of AMPKα subunits (Fig. 2B) and of β1 (data not shown) show a conservation of the regions flanking these sites, indicating that, possibly, these phosphorylation sites have functional roles. Interestingly, T490 was recently found to be an inhibitory phosphorylation site regulated by GSK3 that is involved in metabolic flexibility [36]. We next examined whether mutating these sites to alanine would affect CDK1 phosphorylation of AMPKα2. GST-AMPKα-mutants S377A and T485A combined (AMPKα2-2A) completely blocked ^{32}P labeling on AMPKα by active CDK1/Cyclin B1 complex when compared with wild type (WT) GST-AMPKα (Fig. 2C). After identifying these sites, we generated a phospho-specific antibody for detecting p-S377 and utilized the p-T490 AMPKα1 antibody [36] for detecting p-T485 of AMPKα2. As expected, GST-AMPKα2 WT incubated with activated CDK1/Cyclin B1 displayed high levels of phosphorylation detected with p-S377 and p-T485 antibodies, whereas mutating the two sites to alanine completely abrogated the phospho-signal, confirming the specificity of the phospho-antibodies (Fig. 2D). We also examined if PLK1 is able to phosphorylate AMPK, as one study described regulation of AMPK by PLK1 at T172 during mitosis [37]. We found that PLK1 fails to phosphorylate either of our mitotic sites and both CDK1 and PLK1 were unable to phosphorylate T172 directly (Fig. 2D).

Similarly, *in vitro* kinase assays were performed to determine whether CDK1 can directly phosphorylate AMPKβ1, with GST-tagged AMPKβ1 as substrate. Lysates of mitotically arrested cells robustly phosphorylated AMPKβ1, with RO-3306 inhibition of CDK1 significantly reducing phosphorylation of GST-AMPKβ1 (Fig. 2E). Next, the phosphorylation sites of T19 and S40 were identified on AMPKβ1 that matched the CDK1 consensus motif and likewise were hits in large-scale phosphoproteomic studies [33-35]. Interestingly, in line with our observations in Fig. 1A, indicating that AMPKβ1, but not AMPKβ2, is phosphorylated, both T19 and S40 do not exist in AMPKβ2. *In vitro* kinase assays with activated CDK1/Cyclin B1 complex displayed clear phosphorylation of WT GST-AMPKβ1. Interestingly, the AMPKβ1 T19A and 2A mutations blocked all ^{32}P incorporation at both T19 and S40, possibly indicating lack of T19 phosphorylation precludes S40 phosphorylation, but not vice versa (Fig. 2F). Next, we generated a phospho-specific antibody towards pT19 and found that both AMPKβ1 WT and S40A were clearly phosphorylated at T19 compared to the T19A and 2A mutants (Fig. 2G), once again showing that T19A could be considered identical to 2A.

AMPK is phosphorylated in cells in a CDK1-dependent manner

After confirming AMPK phosphorylation by CDK1 *in vitro*, we next examined this phosphorylation in cells. Immunoprecipitation of endogenous AMPKα2 from HeLa cells treated with nocodazole or with nocodazole plus RO-3306 showed an increase and a loss of S377 phosphorylation respectively (Fig. 3A). Over expressed Flag-AMPKα2 WT, S377A, and T485A constructs transfected into 293T cells treated with or without nocodazole, when Flag-immunoprecipitated, revealed increased S377 phosphorylation for WT α2 under nocodazole treatment and, unsurprisingly, a complete loss in the S377A mutant. Of note, mutating T485 to alanine does not perturb the phosphorylation at S377 (Fig. 3B). These data indicate that AMPKα is phosphorylated at S377 in cells during nocodazole-induced mitotic arrest in a CDK1-dependent manner. Next, to

determine if the β1 subunit was also phosphorylated in cells, we performed Flag-immunoprecipitation of WT and T19A mutant AMPKβ1 from nocodazole-arrested cell lysates and probed them using the phospho-specific AMPKβ1 T19 antibody. Indeed, the phosphorylation signal was potently increased for WT AMPKβ1 in cells arrested in mitosis, but completely absent in the T19A mutant (Fig. 3C). Subsequently, we transfected HA-AMPKα1 WT and 2A into 293T cells and immunoprecipitated HA-AMPKα1 from cells treated with either DMSO, taxol, or nocodazole. The phosphorylation of WT HA-AMPKα1 was found to be increased under taxol and nocodazole arrest, but entirely lost in the 2A mutant (Fig. 3D). To further confirm this as a CDK1-mediated phosphorylation in cells, we immunoprecipitated HA-AMPKα1 WT and 2A from cells treated with nocodazole or with nocodazole plus RO-3306. We detected an increase of T490 phosphorylation with nocodazole treatment which could be largely abolished with the CDK1 inhibitor, RO3306, as well as a complete block of this phosphorylation in the HA-AMPKα1 2A mutant (Fig. 3E). Furthermore, enhanced expression of constitutive active Cyclin B1 promoted AMPK phosphorylation at T490 (α1), S377 (α2), and T19 (β1) (Fig. 3F, G).

Next, we wanted to ascertain if any of the mitotic phosphorylations were essential for AMPK subunit molecular interaction. For this, we co-expressed Myc-AMPKγ1 with either WT or 2A HA-AMPKα1 and WT or T19A Flag-AMPKβ1 in 293T cells, then treated with or without nocodazole and co-immunoprecipitated by pulling down HA-AMPKα1. Our results showed that neither of the phospho-null mutations in α1 or β1 had any deleterious effect on subunit interaction (Fig. 3H). AMPK has several autophosphorylation sites [38-40], so we wanted to determine if AMPK mitotic phosphorylation at S377 was either due to autophosphorylation or if AMPK kinase activity was required via feedback mechanisms for the S377 mitotic phosphorylation to occur. To do this, we transfected WT and kinase-dead (K45R) HA-AMPKα2 in 293T cells, which were treated with or without nocodazole, and then examined the levels of p-S377 (Fig. 3I). We found there was no

difference between the WT and K45R mutant for AMPKα2 S377 mitotic phosphorylation, indicating that this is not an autophosphorylation site and that AMPK kinase activity is not a precondition for S377 mitotic phosphorylation. Overall, these data provide an argument that CDK1 phosphorylates multiple AMPK subunits in cells during mitosis.

We collected samples from a double thymidine block and release and determined the phospho-status of AMPK. p-S377 signal was increased when cells enter into mitosis (8-10 hours being released from double thymidine block) (Fig. 3J). Very weak signals were detected in interphase or cytokinesis cells in freely cycling (Fig. 3K, yellow arrows). The phospho-signal was significantly increased in cells in mitosis (Fig. 3K, white arrows). These observations indicates that phosphorylation of AMPK S377 occurs during normal mitosis.

AMPK regulates mitotic progression

After we had ascertained AMPK mitotic phosphorylation is mediated by CDK1, we wanted to explore AMPK's possible role in regulating mitotic processes through gene knockout phenotypic analysis. We generated an AMPKα1/α2 double knockout (AMPKα-KO) and as well as an AMPKβ1 knockout in U2OS cells using a CRISPR-Cas9 approach. In the AMPKα-KO, not only was AMPKα1 and α2 expression completely absent, but also both the AMPKβ subunit protein levels were severely diminished, indicating a need for AMPKα subunits for stability of the other complex members (Fig. 4A). In the AMPKβ1-KO cell line, aside from AMPKβ1 protein expression being completely lost, AMPKβ2 and AMPKα1/α2 expression remained unchanged (Fig. 4B). Next, we took U2OS and U2OS AMPKα-KO cells, arrested them at metaphase with nocodazole, and then released the rounded-up mitotic cells in fresh media. Upon release, we harvested cells at the indicated time points and probed with Cyclin B1, CDC25C, and CDC27 to detect the rate of mitotic exit of each cell line. No noticeable differences were seen in the rates of degradation of Cyclin B1

or dephosphorylation of CDC25C and CDC27 between U2OS AMPKα-KO and controls (Fig. 4C). Subsequently, by way of fluorescent live-cell imaging, we examined mitotic entry and progression of parental and AMPKα-KO U2OS cells stably expressing RFP-H2B. The parental U2OS cells quickly condensed their chromatin and aligned their chromosomes in a tightly packed metaphase plate within 15 minutes. Anaphase onset occurred 35 minutes after nuclear-envelope break down (NEBD), with telophase, measured by chromatin decondensation, occurring at 50 minutes post-NEBD (Fig. 4D upper). AMPKα-KO cells, in contrast, have a marked delay in aligning their chromosomes at metaphase, approximately 115 minutes after NEBD, and a postponement of anaphase onset to 120 minutes post-NEBD (Fig. 4E lower). Quantitative analysis revealed that AMPKα-KO cells had 77% longer mitotic (NEBD to anaphase) lengths than controls (Fig. 4F). Unsurprisingly, AMPKα-KO cells had a significantly longer mitotic length, which concurs with a previous live-cell study using bright field microscopy that specified a significantly increased mitotic length for AMPK siRNA-treated HeLa cells [15]. Of note, similar anaphase to telophase timing in U2OS control and AMPKα-KO reinforces our earlier observation of unhindered mitotic exit in these cells (Fig. 4D-F). We noticed fewer rounded-up cells in the AMPKα-KO and AMPKβ1-KOs when treated with taxol or nocodazole, so we performed cell cycle analysis using propidium iodide and found that there was no significant difference in the percentages of mitotically arrested cells between the knockouts and the controls (Supplemental Figure 1). Next we stained U2OS control, AMPKα-KO and AMPKβ1-KOs cells (treated with or without nocodazole for 0, 8, 16, or 24 hours) with fluorescently labeled phospho-Histone H3 (S10) antibody to measure the mitotic index. Surprisingly, the number of mitotic cells in AMPKα-KO and AMPKβ1-KO U2OS, when treated for 16 or 24 hours with nocodazole, was significantly lower than that of parental U2OS, indicating these cells may not be entering mitosis, but, having completed S-phase, have 4N DNA content (Fig. 4G).

Pharmacological abrogation of AMPK activity through use of small molecule inhibitors has been used widely for the study of AMPK function [15, 17, 18, 41]. We utilized the Compound C and a newly identified AMPK-specific inhibitor SBI-0206965, which has been demonstrated to have an entirely different set of potential off-target kinases inhibited compared to Compound C [42]. Abrupt inhibition of AMPK in RFP-H2B-expressing U2OS cells was accomplished with treatment with 5 μM SBI-0206965 or 5 μM Compound C, which were then immediately imaged for 24 hours and the timing of each mitotic phase was analyzed. Similar to AMPKα-KO cells, cells in which AMPK activity was inhibited displayed distinctly increased metaphase lengths (Fig. 5A, B), demonstrating the importance of AMPK kinase activity for timely mitotic progression. From this, we wanted to further investigate why these cells were getting delayed at metaphase. Examination via confocal microscopy of U2OS cells with either genetic or pharmacological nullification of AMPK kinase function revealed that a vast majority of AMPKα-KOs or U2OS cells treated with Compound C fail to properly align their chromosomes during metaphase (Fig. 5C). Representative images are shown in (Fig. 5D), displaying misaligned chromosomes frequently seen as far away from the metaphase plate as the centrosomes. The observed metaphase arrest in cells lacking functioning AMPK could be due to, in part, how chromosomes with kinetochores improperly attached to the mitotic spindle activate the spindle assembly checkpoint (SAC), which delays anaphase sister-chromatid separation until each chromosome is properly aligned and attached to the spindle [43, 44].

AMPK phosphorylation is required for mitotic progression

The necessity for AMPKα expression for mitotic entry and proper prophase to anaphase progression prompted us to investigate the role of the two mitotic CDK1-mediated phosphorylations of AMPKα, S377 and T490. For this, we generated stable cell lines expressing either AMPKα1 WT or AMPKα1 2A in the AMPKα-KO U2OS cells (Fig. 6A), with expression of

AMPKα1 WT or 2A near the levels found in parental U2OS rescuing the expression of both AMPKβ subunits. Measurement of the mitotic index of U2OS AMPKα-KO cells treated with nocodazole, once again, revealed a concomitant drop in cells arrested in mitosis which lack AMPK expression. This could be fully rescued by the expression of AMPKα1 WT, but only partially by the mitotic phosphorylation-null α1-2A (Fig. 6B), indicating that AMPKα1 could be the primary mitotic subunit in these cells and that mitotic phosphorylation by CDK1 may be important for proper progression into mitosis. We also created AMPKα2-WT, AMPKα1-K45R (kinase-dead), and AMPKα1-T183A (phospho-activation-null) add-backs to the AMPKα-KO background (Fig. 6C). Expression of each form of α-subunit were sufficient for recovering the expression of both AMPKβ subunits (Fig. 6C). Analysis of the mitotic index of the α1-K45R and α1-T183A mutants, showed the same significant decrease in mitotic cells as seen with AMPKα-KO (Fig. 6D), demonstrating that both AMPK kinase activity and activation at T183 are required for mitotic arrest. AMPKα2-WT expression was only able to partially increase the suppressed phosphorylation of S10 on histone H3 (Fig. 6B). We next sought to elucidate the roles played by AMPK mitotic phosphorylation, kinase activity, and phospho-activation in mitotic progression by stably expressing RFP-H2B in each AMPKα1 mutant and the AMPKβ1-KO cell lines, following unperturbed mitoses, and determining the timing of mitotic entry to anaphase onset. Interestingly, AMPKα1-WT and α1-T183A could fully rescue the prometaphase delay seen in AMPKα-KO cells (Fig. 6E). In addition, knocking out AMPKβ1 had no effect on metaphase alignment or the interval from NEBD to anaphase. Contrastingly, α1-K45R could not rescue and AMPKα1-2A could only partially rescue the prolonged arrest during prometa/metaphase (Fig. 6E), indicating that AMPK kinase activity is required, and CDK1 mitotic phosphorylation is, at least in part, essential for proper early mitotic progression. Since we saw that the AMPKα-KOs, when treated for 16 hours with nocodazole, were indeed accumulating with 4N DNA content and were pH3 (S10)-negative, we then wanted to confirm whether these cells were endoreduplicating or simply never entering mitosis. To do this, we used fluorescent live-cell microscopy to follow individual cells under the

treatment of taxol or nocodazole for 48 hours. Remarkably, 73-81% of AMPKα-KOs persisted in interphase and never arrested in mitosis, which was significantly higher than parental U2OS in which only 48-49% remained in interphase (Fig. 6F). In contrast, AMPKα1-WT expression partially rescued and cleared more cells to progress into mitosis, so only 49-52% remained unarrested, whereas AMPKα1-2A was more like AMPKα-KO with 68-77% lingering in interphase (Fig. 6F). These data confirmed that CDK1-mediated phosphorylation of, and the kinase activity by, AMPK is not only important for faithful mitotic entry, but also for proper progression to DNA segregation at anaphase.

AMPK phosphorylation regulates transcription of genes involved in mitosis

To get insight into the downstream signaling of AMPK, we next investigated the transcriptome of U2OS cells by next generation RNA sequencing (RNA-seq). Comparative analysis of parental U2OS (control) vs. AMPKα-KO and control vs. AMPKα1-2A was performed using Ingenuity Pathway Analysis (IPA) to examine canonical pathways similarly altered in each to designate effects due to dysregulation of CDK1 phosphosites. Intriguingly, canonical pathways influencing actin dynamics such as actin cytoskeleton signaling, ILK signaling, and regulation of actin-based motility by Rho were predicted to be significantly activated (Fig. 7A). Unsurprisingly, the expression of a multitude of genes involved in promoting cellular movement and migration were increased and several inhibitors of cell movement were diminished in AMPKα-KO and α1-2A cells compared to controls (Fig. 7B). By examining alterations of downstream gene expression, upstream analysis pinpointed numerous possible upstream regulators. Most of the highest-scoring upstream effectors were analogously modulated between AMPKα-KO and α1-2A compared to controls (Fig. 7C), indicating that loss of phosphorylation of AMPK by CDK1 is comparable to AMPK knockout for alterations seen in these particular pathways. We previously detected stark reduction of p-Histone H3 (S10) in both the AMPKα-KO and α1-2A cells, which led

us to speculate that this was possibly due to either phosphatase dysregulation leading to hyper-dephosphorylation, or perturbation of kinase signaling leading to inadequate phosphorylation of Histone H3. Interestingly, there were eight significantly up- or down-regulated phosphatases found to be changed mutually between the AMPKα-KO and α1-2A cells compared to controls (Fig. 7D). Furthermore, between the two treatments, the expression levels of ten kinases and two mitosis-associated kinases significantly changed compared to controls (Fig. 7E).

AMPK phosphorylation potentiates taxol cytotoxicity

Taxanes and similar compounds rely on the disruption of microtubule dynamics in order to arrest cells in mitosis through activation of the SAC, with the prolonged arrest triggering cell death through a unique antiproliferative process called mitotic cell death [45] or through aberrant mitosis and eventual death in G_1 [46]. Because of this method of action, cancer cells must enter mitosis in order to suffer the effects of taxol and eventually succumb to cell death mechanisms. With this in mind, we next had to ascertain if loss of AMPK activity could indeed provide cancer cells with a means to resist cell death by taxol treatment. AMPKα-KO cells, compared to parental U2OS, had distinctly reduced levels of apoptosis revealed by cleaved PARP. Addition of AMPKα1-WT amply rescued and resensitized the cells, whereas AMPKα1-2A had muted levels of cleaved PARP similar to AMPKα-KO (Fig. 8A), suggesting that cells lacking AMPKα expression have a proclivity to resist taxol-mediated mitotic cell death. Similar resistance was seen in MCF7 and SKBR3 breast adenocarcinoma cells when treated concomitantly with taxol or vinblastine (a microtubule destabilizing agent) and SBI-0206965. Both cell types displayed high cleaved PARP protein levels under taxol or vinblastine treatment alone. Yet, when AMPK was inhibited in MCF7 and SKBR3 cells exposed to these drugs for 24 hours, substantial reductions in cleaved PARP were seen (Fig. 8B), evidencing that AMPK activity is necessary for significant levels of apoptosis elicited by antitubulin mitotic arrest. Both SBI-0206965 and Compound C could significantly

reduce the mitotic index of HeLa cells that were treated with taxol compared to taxol treatment alone (Fig. 8C, D), signifying that the lack of apoptosis in these cells is possibly due to AMPK inhibition blocking mitotic entry and thus protecting cancer cells from mitotic cell death and apoptosis triggered by paclitaxel. Survival curves for breast cancer patients who received systemic treatments and who had high AMPKα1 expression displayed significantly higher relapse-free survival (RFS) rates than survival curves for patients who had low AMPKα1 expression [47] (Fig. 8E). Interestingly, there is no difference in RFS for patients with high or low AMPKα2 or AMPKβ2, but a moderately higher RFS rate in high AMPKβ1-expressing patients (Fig. 8F-H).

DISCUSSION

AMPK has previously been reported to have increased phosphorylation levels at the T172 activation site during mitosis [14, 15, 17, 20, 48]. The current study is the first to identify direct phosphorylation sites outside of T172 on the AMPK complex, targeted by a bona fide mitotic kinase. These phosphorylations by CDK1 on the AMPKα1, α2, and β1 subunits, seen *in vitro* and in cells, adds a novel upstream kinase to the group of known AMPK phospho-regulators. CDK1 phosphorylation of AMPKα2 at S377/T485 and AMPKα1 at T490, as well as of AMPKβ1 at T19, was seen to be highly enriched in cells arrested in mitosis by anti-mitotic drugs, which could be abolished by addition of CDK1-specific inhibitors. The reduced mitotic index in AMPKα-KOs cells when treated with taxol or nocodazole was, interestingly, due to their lack of mitotic entry when individual cells were monitored using live-cell imaging. This could be rescued by reconstitution of α1 WT, but not α1 2A, providing evidence that AMPK activity and CDK1 phosphorylation is important for cellular entry into mitosis. It has been reported that AMPK phosphorylation of GBF1 is required for mitotic entry though regulation of mitotic Golgi fragmentation [17, 18], so it may be

through this process or through other, as of yet undiscovered, means by which AMPK phosphorylation by CDK1 promotes mitotic entry.

The IPA analysis of RNA-seq data of AMPKα-KO and α1-2A cells compared to controls revealed multiple pathways, functions, and upstream effectors which are modified by loss of CDK1 phospho-regulation. From this, the predicted activation of mitogen-activated protein kinase 1 (MAPK1) could conceivably be driven through stimulation of actin cytoskeleton signaling [49]. Furthermore, the spleen tyrosine kinase (SYK) and interferon gamma (IFNG) downregulation similarly seen in both knockout and CDK1 phosphorylation-null AMPK cells is of importance due to each gene's role in suppression of tumorigenesis in breast carcinoma [50] and promotion of apoptosis [51], respectively. Stimulation of amphiregulin (AREG) signaling is of note because it promotes cancer growth through interactions with EGF/TGFα receptors [52]. Likewise, high SWI/SNF-related matrix-associated actin-dependent regulator of chromatin 4 (SMARC4) activity has been seen to promote tumor cell proliferation and is associated with poor prognosis in multiple cancers [53, 54] and has been reported to increase expression of CD44 [55], itself a promoter of resistance to apoptosis and important in breast cancer cell migration [56, 57]. Additionally, overactive tumor protein 73 (TP73) has also been implicated in poor clinical behavior and in promotion of tumorigenesis of breast carcinomas [58]. Interestingly, estrogen receptor 1 (ERSR1) upregulation has been associated with EZH2 downregulation [59], both of which are seen to occur in AMPKα knockout and mitotic phosphorylation-null AMPKα1-2A cells. High estrogen receptor (ER) expression has been associated with increased proliferation and higher grade breast cancer [60]. Androgen receptor (AR) overexpression in triple-negative breast cancers can allow a switch from ER-dependence to AR-dependence which results in resistance to aromatase inhibitor treatments [61]. Further, phosphatases which are increased in late-stage and aggressive triple-negative breast cancers such as ALPL and PTP4A3 have been found to be indicative of poor patient survival and have been discovered as promoters of cancer cell proliferation [62, 63].

Importantly, suppression of DUSP5 expression is correlated with paclitaxel resistance and poor prognosis in basal-like breast cancer [64].

Other studies have shed some light on AMPK's role in mitosis through chemically inhibiting AMPK kinase activity. Compound C, a widely used AMPK inhibitor, has been shown to delay mitotic entry [17, 18], cause spindle misorientation and misattachment of chromosomes through actin bundling, and to increase mitotic length as measured from mitotic rounding to cytokinesis via bright field microscopy [15, 41]. Correspondingly, we found that nullification of AMPK kinase activity by Compound C or a newly described AMPK-specific inhibitor, SBI-0206965 [42], results in significantly delayed progression through mitosis from NEBD to anaphase and is marked by a profound degree of chromosomal misalignment. Our results have also shown that AMPK inhibitors can constrain the killing ability of antitubulin drugs in breast cancer cells through blocking mitotic entry. This is significant because cells must proceed into mitosis in order for the mechanism of taxol microtubule stabilization to lead to mitotic arrest and eventual cell death, indicating that in breast cancer patients, use of AMPK inhibitors is contraindicated.

Metformin, the common antidiabetic drug for treating Type 2 diabetes and activator of AMPK, has been shown to cause cell cycle arrest, suppress anchorage-depended growth, and inhibit cell proliferation in breast cancer cell lines [65-67]. Additional studies suggest that metformin may improve the efficacy of breast cancer treatments and regimens as well as selectively target and kill cancer stem cells [14, 68, 69]. Metformin has also been shown to constrain mammary tumor expansion in mice [70]. This fact has led to the dozens of clinical trials exploring the use of metformin as a neoadjuvant, in combinatorial chemotherapies or as a chemoprevention agent [71]. Indeed, several clinical Phase II and Phase III trials have recently been initiated to examine the synergistic effects of treatment with metformin and other drugs used in cytotoxic chemotherapy, such as docetaxel or paclitaxel. These were initiated after meta-analysis of retrospective studies identified the use of metformin with a significant reduction in cancer-related

mortality for patients [72, 73]. Our analysis of patient data revealed that breast cancer patients who had high AMPKα1 or AMPKβ1 expression and received systemic treatments displayed significantly higher RFS rates than patients who had low AMPKα1 or AMPKβ1 expression, respectively [47]. This strongly indicates the use of metformin in breast cancer treatment regimens, especially in patients with tumors expressing low levels of the mitotically phosphorylated AMPK subunits, AMPKα1 and β1, in order to improve their survival.

In conclusion, we propose that CDK1 regulates AMPK control of mitotic entry and progression. It remains to be determined which signaling networks or processes CDK1-phosphorylated AMPK utilizes to drive these events. Thus, future studies will need to examine whether this newly identified CDK1/AMPK axis is involved in Golgi fragmentation, mitotic spindle orientation, or some other currently unassociated mitotic process.

MATERIALS & METHODS

Cell culture and transfection

HEK293T, HeLa, U2OS, MCF7, and SKBR3 cell lines were purchased from American Type Culture Collection (ATCC) and cultured as ATCC instructed. The cell lines were authenticated at ATCC and were used at low (< 25) passages. Attractene (Qiagen) was used for transient overexpression of proteins in HEK293T cells following the manufacturer's instructions. Lentivirus packaging, infection, and subsequent selection were done as we have described previously [74]. Nocodazole (100 ng/mL for 16 h) and taxol (100 nM for 16 h) (Selleck Chemicals) were used to arrest cells in mitosis unless otherwise indicated. Kinase inhibitors were purchased from Selleck Chemicals (VX680, BI2536, Purvalanol A, SP600125, SB216736, SBI-0206965, and MK-2206), ENZO life Sciences (RO3306), or LC Laboratory (U0126 and SB203580). All other chemicals were from either from Sigma or Thermo Fisher.

Expression Constructs

Human pcDNA3-HA-AMPKα1-WT and Myc-AMPKγ1-WT constructs were a gift from Dr. Ken Inoki [75]. Human pECE-HA-AMPKβ1-WT and pECE-HA-AMPKα2-WT were gifts from Anne Brunet (Addgene plasmid # 31666 and 31654) [20]. pLKO.1-H2B-RFP was a gift from Elaine Fuchs (Addgene plasmid # 26001) [76]. Point mutations were generated by the QuikChange Site-directed PCR mutagenesis kit (Stratagene) and verified by sequencing. Retroviral expression constructs were made by cloning full-length AMPKβ1 or AMPKα2 cDNA into MaRX^{TM}IV [77]. Lentiviral expression constructs were generated by cloning full length AMPKα2 cDNAs into pSIN4-Flag-IRES-Puro or AMPKα1 into pSIN4-Flag-IRES-Neo [32].

EGFP-expressing all-in-one CRISPR construct

To construct the all-in-one CRISPR/Cas9n plasmid targeting AMPKβ1, the sense and anti-sense oligonucleotides from Supplemental Table 1 were synthesized, annealed, and Golden Gate assembled into the pX330A_D10A-1x2-EGFP and pX330S-2 vectors as described previously [32]. After the two vectors were generated, a final Golden Gate assembly was performed to generate the all-in-one vector as described previously [78]. The resulting pX330A_D10A-1x2-EGFP-PRKAB1-AB construct was transfected into cells and GFP-positive clones were selected by flow cytometry-based cell sorting.

To construct the all-in-one CRISPR/Cas9n plasmid targeting both AMPKα1 and α2, the sense and anti-sense oligonucleotides from Table 1B were synthesized, annealed, and Golden Gate assembled into the pX330A_D10A-1x2-EGFP, pX330S-2, pX330S-3, and pX330S-4. After the four vectors were generated, a final Golden Gate assembly was performed to generate the all-in-

one vector. The resulting pX330A_D10A-1x2-EGFP-PRKAA1/2-ABCD construct was transfected into cells and GFP-positive clones were selected by flow cytometry-based cell sorting.

Recombinant protein purification and in vitro kinase assay

GST-tagged AMPKα2-WT and 2A, as well as GST-tagged AMPKβ1-WT, T19A, S40A, and 2A were cloned in pGEX-5X-1. Proteins were bacterially expressed and purified on GSTrap FF affinity columns (GE Healthcare) following the manufacturer's instructions. GST-AMPKα2 or GST-AMPKβ1 (0.5–1 μg) was incubated with 10 U recombinant CDK1/cyclin B complex (New England Biolabs) or 100 ng CDK1/cyclin B (SignalChem) in kinase buffer (New England Biolabs) in the presence of 5 μCi γ-^{32}P-ATP (3000 Ci/mmol, PerkinElmer). PLK1 kinase was also obtained from SignalChem. Phosphorylation was visualized by autoradiography (^{32}P incorporation) followed by Western blotting or detected by phospho-specific antibodies.

Antibodies

Rabbit polyclonal antibody against p-T485/T490 AMPKα1/2 was a gift from Dr. Ken Inoki [36]. AMPKα1, AMPKα2, AMPKβ1, AMPKβ2, AMPKγ1, AMPKγ2, AMPKγ3, AMPKα1/α2, p-AMPKα (T172), p-AMPKβ1 (S182), p-AMPKβ1 (S108), p-Aurora A/B/C (T288/T232/T198), CDC25C, p-Histone H3 (S10) Alexa Fluor® 488, and cleaved PARP antibodies were from Cell Signaling Technology. Anti-β-Actin, Cyclin B1 and CDC27 antibodies were from Santa Cruz Biotechnology. Flag, HA, and Myc antibodies were from Sigma. α-Tubulin antibody was from Abcam. γ-Tubulin antibody was from Biolegend. p-AMPKα2 (S377) and p-AMPKβ1 (T19) phospho-antibodies were generated and purified by AbMart. The phospho-peptides used for immunizing rabbits were PLIAD-pS-PKARC (p-AMPKα2 S377) and HGGHK-pT-PRRDS (p-AMPKβ1 T19). Matching non-phosphorylated peptides were also synthesized and used for antibody purification and blocking assays.

Immunoprecipitation, Phos-tag™, and Western blot analysis

Phos-tag™ was obtained from Wako Pure Chemical Industries, Ltd. (cat#: 304-93521). Phos-tag™ gels were made using 10 μM Phos-tag™ (with 100 μM $MnCl_2$) in 8% SDS-acrylamide gels as described [79]. Immunoprecipitation, western blotting, and lambda phosphatase treatment assays were done as previously described [80].

Immunofluorescence staining and confocal microscopy

Cell fixation, permeabilization, immunofluorescence staining, and confocal microscopy were done as previously described [81].

RNA extraction, construction of RNA libraries, and RNA-Seq

We extracted the RNA using the Direct-zol™ RNA Miniprep Plus Kit (Zymo Research) and evaluated the purity and concentration of the RNA by ultraviolet spectroscopy (NanoDrop). RNA integrity numbers (RIN) were evaluated using the Agilent 2100 Bioanalyzer. RNA sequencing libraries were constructed using 1000 ng of total RNA from each sample and the TruSeqV2 kit from Illumina following manufacturer's protocol. Illumina NextSeq sequencing and NGS data acquisition were conducted at the UNMC Genomics Core Facility. The libraries were subjected to 75 bp paired-end high-output sequencing using a NextSeq500 sequencer to generate approximately 33.3 to 41.6 million reads per sample. Fastq files were generated using the bc12fastq software, version 1.8.4 and provided to the UNMC Bioinformatics Core facility for further analysis. The original fastq format reads were trimmed and filtered using the fqtirm tool (https://ccb.jhu.edu/software/fqtrim) to remove adapters, terminal unknown bases (Ns) and low quality 3' regions (Phred score < 30). The trimmed fastq files were processed by our facility's newly developed standard pipeline utilizing STAR [82] as the aligner and RSEM [83] as the tool for annotation and quantification at both gene and isoform levels. TPM values were used for comparison results (student's t-test) for all the available genes. The Benjamini-Hochberg (BH)

adjusted p values [84] were also provided to adjust for multiple testing-caused false discovery rate (FDR) with significant level of adjusted p value of ≤ 0.05.

Live-Cell Imaging

U2OS and lentiviral-transduced U2OS were plated on black 96-well optical bottom plates (Thermo Fisher). Live-cell imaging was performed in a Cellomics Arrayscan VTI HCS Reader with 37 °C, 5% CO_2 incubation using FluroBrite DMEM (Thermo Fisher) supplemented with 4 mM L-glutamine, 10% FBS, 1% Pen/Strep. Cells were monitored for 24 h and pictures were taken every 5 min using an RFP filter. Measurements of cell cycle durations were done using the time-lapse sequences.

Statistical analysis

Statistical significance was analyzed using a two-tailed, unpaired Student's t-test or using a two-way ANOVA with the Šidák correction for multiple comparisons. A P value of < 0.05 was considered to indicate statistical significance.

ACKNOWLEDGMENTS

We are very grateful to Dr. Ken Inoki (University of Michigan) for the p-AMPKα1/2 T490/T485 antibody and AMPK constructs. Dr. Shuping Yang (Shandong University) helped generate the AMPKα1-2A mutant. All fluorescence images were acquired by Zeiss LSM 710 or LSM 800 confocal microscopes at the Advanced Microscopy Core at the University of Nebraska Medical Center. The core is supported in part by grant P30 GM106397 from the National Institutes of Health (NIH). RNA sequencing was performed at University of Nebraska DNA Sequencing Core. The core receives partial support from the National Institute for General Medical Science (NIGMS) INBRE - P20GM103427-14 and COBRE - 1P30GM110768-01 grants as well as The Fred & Pamela Buffett Cancer Center Support Grant - P30CA036727. Research in the Dong laboratory is supported by Fred & Pamela Buffett Cancer Center Support Grant (P30 CA036727), grants P30 GM106397 and R01 GM109066 from the NIH. We also thank Dr. Joyce Solheim for critical reading and comments on the manuscript.

AUTHOR CONTRIBUTIONS

SS and JD designed and wrote the paper. SS, YZ, MS, JZ, and YC performed the experiments, analyzed the data and interpreted the results. YC also provided technical support. All authors reviewed and approved the manuscript prior to submission.

REFERENCES

1. Bakhoum, S.F. and C. Swanton, *Chromosomal instability, aneuploidy, and cancer.* Front Oncol, 2014. **4**: p. 161.
2. Nowak, M.A., et al., *The role of chromosomal instability in tumor initiation.* Proc Natl Acad Sci U S A, 2002. **99**(25): p. 16226-31.
3. Pino, M.S. and D.C. Chung, *The chromosomal instability pathway in colon cancer.* Gastroenterology, 2010. **138**(6): p. 2059-72.
4. Schvartzman, J.M., R. Sotillo, and R. Benezra, *Mitotic chromosomal instability and cancer: mouse modelling of the human disease.* Nat Rev Cancer, 2010. **10**(2): p. 102-15.
5. Kops, G.J., D.R. Foltz, and D.W. Cleveland, *Lethality to human cancer cells through massive chromosome loss by inhibition of the mitotic checkpoint.* Proc Natl Acad Sci U S A, 2004. **101**(23): p. 8699-704.
6. Rao, C.V. and H.Y. Yamada, *Genomic instability and colon carcinogenesis: from the perspective of genes.* Front Oncol, 2013. **3**: p. 130.
7. Kops, G.J., B.A. Weaver, and D.W. Cleveland, *On the road to cancer: aneuploidy and the mitotic checkpoint.* Nat Rev Cancer, 2005. **5**(10): p. 773-85.
8. Reiter, R., et al., *Aurora kinase A messenger RNA overexpression is correlated with tumor progression and shortened survival in head and neck squamous cell carcinoma.* Clin Cancer Res, 2006. **12**(17): p. 5136-41.
9. Shichiri, M., et al., *Genetic and epigenetic inactivation of mitotic checkpoint genes hBUB1 and hBUBR1 and their relationship to survival.* Cancer Res, 2002. **62**(1): p. 13-7.
10. Manchado, E., M. Guillamot, and M. Malumbres, *Killing cells by targeting mitosis.* Cell Death Differ, 2012. **19**(3): p. 369-77.
11. Mihaylova, M.M. and R.J. Shaw, *The AMPK signalling pathway coordinates cell growth, autophagy and metabolism.* Nat Cell Biol, 2011. **13**(9): p. 1016-23.
12. Zadra, G., J.L. Batista, and M. Loda, *Dissecting the Dual Role of AMPK in Cancer: From Experimental to Human Studies.* Mol Cancer Res, 2015. **13**(7): p. 1059-72.
13. Lee, J.H., et al., *Energy-dependent regulation of cell structure by AMP-activated protein kinase.* Nature, 2007. **447**(7147): p. 1017-20.
14. Vazquez-Martin, A., et al., *AMPK: Evidence for an energy-sensing cytokinetic tumor suppressor.* Cell Cycle, 2009. **8**(22): p. 3679-83.
15. Thaiparambil, J.T., C.M. Eggers, and A.I. Marcus, *AMPK regulates mitotic spindle orientation through phosphorylation of myosin regulatory light chain.* Mol Cell Biol, 2012. **32**(16): p. 3203-17.
16. Vazquez-Martin, A., et al., *Polo-like kinase 1 directs the AMPK-mediated activation of myosin regulatory light chain at the cytokinetic cleavage furrow independently of energy balance.* Cell Cycle, 2012. **11**(13): p. 2422-6.
17. Mao, L., et al., *AMPK phosphorylates GBF1 for mitotic Golgi disassembly.* J Cell Sci, 2013. **126**(Pt 6): p. 1498-505.
18. Lee, I.J., C.W. Lee, and J.H. Lee, *CaMKKβ-AMPKα2 signaling contributes to mitotic Golgi fragmentation and the G2/M transition in mammalian cells.* Cell Cycle, 2015. **14**(4): p. 598-611.
19. Domenech, E., et al., *AMPK and PFKFB3 mediate glycolysis and survival in response to mitophagy during mitotic arrest.* Nat Cell Biol, 2015. **17**(10): p. 1304-16.

20. Banko, M.R., et al., *Chemical genetic screen for AMPKα2 substrates uncovers a network of proteins involved in mitosis.* Mol Cell, 2011. **44**(6): p. 878-92.
21. Ito, M., et al., *Myosin phosphatase: structure, regulation and function.* Mol Cell Biochem, 2004. **259**(1-2): p. 197-209.
22. Peters, J.M., *The anaphase promoting complex/cyclosome: a machine designed to destroy.* Nat Rev Mol Cell Biol, 2006. **7**(9): p. 644-56.
23. Tuazon, P.T. and J.A. Traugh, *Activation of actin-activated ATPase in smooth muscle by phosphorylation of myosin light chain with protease-activated kinase I.* J Biol Chem, 1984. **259**(1): p. 541-6.
24. Mirouse, V., et al., *LKB1 and AMPK maintain epithelial cell polarity under energetic stress.* J Cell Biol, 2007. **177**(3): p. 387-92.
25. Sanli, T., et al., *Ionizing radiation activates AMP-activated kinase (AMPK): a target for radiosensitization of human cancer cells.* Int J Radiat Oncol Biol Phys, 2010. **78**(1): p. 221-9.
26. Sanli, T., et al., *Ionizing radiation regulates the expression of AMP-activated protein kinase (AMPK) in epithelial cancer cells.* Radiotherapy and Oncology, 2012. **102**(3): p. 459-465.
27. Nakano, A., et al., *AMPK controls the speed of microtubule polymerization and directional cell migration through CLIP-170 phosphorylation.* Nat Cell Biol, 2010. **12**(6): p. 583-90.
28. Sun, X., et al., *Microtubule-binding protein CLIP-170 is a mediator of paclitaxel sensitivity.* J Pathol, 2012. **226**(4): p. 666-73.
29. Dasgupta, B. and J. Milbrandt, *AMP-activated protein kinase phosphorylates retinoblastoma protein to control mammalian brain development.* Dev Cell, 2009. **16**(2): p. 256-70.
30. Tripodi, F., et al., *Snf1/AMPK is involved in the mitotic spindle alignment in Saccharomyces cerevisiae.* Sci Rep, 2018. **8**(1): p. 5853.
31. Zhang, L., et al., *CDK1 phosphorylation of TAZ in mitosis inhibits its oncogenic activity.* Oncotarget, 2015. **6**(31): p. 31399-412.
32. Stauffer, S., et al., *CDK1-mediated mitotic phosphorylation of PBK is involved in cytokinesis and inhibits its oncogenic activity.* Cell Signal, 2017. **39**: p. 74-83.
33. Daub, H., et al., *Kinase-selective enrichment enables quantitative phosphoproteomics of the kinome across the cell cycle.* Mol Cell, 2008. **31**(3): p. 438-48.
34. Dulla, K., et al., *Quantitative site-specific phosphorylation dynamics of human protein kinases during mitotic progression.* Mol Cell Proteomics, 2010. **9**(6): p. 1167-81.
35. Dephoure, N., et al., *A quantitative atlas of mitotic phosphorylation.* Proceedings of the National Academy of Sciences, 2008. **105**(31): p. 10762-10767.
36. Suzuki, T., et al., *Inhibition of AMPK catabolic action by GSK3.* Mol Cell, 2013. **50**(3): p. 407-19.
37. Vazquez-Martin, A., et al., *Polo-like kinase 1 regulates activation of AMP-activated protein kinase (AMPK) at the mitotic apparatus.* Cell Cycle, 2011. **10**(8): p. 1295-302.
38. Oligschlaeger, Y., et al., *The recruitment of AMP-activated protein kinase to glycogen is regulated by autophosphorylation.* J Biol Chem, 2015. **290**(18): p. 11715-28.
39. Woods, A., et al., *Identification of phosphorylation sites in AMP-activated protein kinase (AMPK) for upstream AMPK kinases and study of their roles by site-directed mutagenesis.* J Biol Chem, 2003. **278**(31): p. 28434-42.

40. Mitchelhill, K.I., et al., *Posttranslational modifications of the 5'-AMP-activated protein kinase beta1 subunit.* J Biol Chem, 1997. **272**(39): p. 24475-9.
41. Wei, C., et al., *The LKB1 tumor suppressor controls spindle orientation and localization of activated AMPK in mitotic epithelial cells.* PLoS One, 2012. **7**(7): p. e41118.
42. Dite, T.A., et al., *AMP-activated protein kinase selectively inhibited by the type II inhibitor SBI-0206965.* J Biol Chem, 2018. **293**(23): p. 8874-8885.
43. Lara-Gonzalez, P., F.G. Westhorpe, and S.S. Taylor, *The spindle assembly checkpoint.* Curr Biol, 2012. **22**(22): p. R966-80.
44. Musacchio, A. and E.D. Salmon, *The spindle-assembly checkpoint in space and time.* Nat Rev Mol Cell Biol, 2007. **8**(5): p. 379-93.
45. Vitale, I., et al., *Mitotic catastrophe: a mechanism for avoiding genomic instability.* Nat Rev Mol Cell Biol, 2011. **12**(6): p. 385-92.
46. Abal, M., J.M. Andreu, and I. Barasoain, *Taxanes: microtubule and centrosome targets, and cell cycle dependent mechanisms of action.* Curr Cancer Drug Targets, 2003. **3**(3): p. 193-203.
47. Gyorffy, B., et al., *An online survival analysis tool to rapidly assess the effect of 22,277 genes on breast cancer prognosis using microarray data of 1,809 patients.* Breast Cancer Res Treat, 2010. **123**(3): p. 725-31.
48. Pinter, K., et al., *Subunit composition of AMPK trimers present in the cytokinetic apparatus: Implications for drug target identification.* Cell Cycle, 2012. **11**(5): p. 917-21.
49. Hoffman, L., et al., *Mechanical signals activate p38 MAPK pathway-dependent reinforcement of actin via mechanosensitive HspB1.* Mol Biol Cell, 2017. **28**(20): p. 2661-2675.
50. Coopman, P.J., et al., *The Syk tyrosine kinase suppresses malignant growth of human breast cancer cells.* Nature, 2000. **406**(6797): p. 742-7.
51. Ruiz-Ruiz, C., C. Munoz-Pinedo, and A. Lopez-Rivas, *Interferon-gamma treatment elevates caspase-8 expression and sensitizes human breast tumor cells to a death receptor-induced mitochondria-operated apoptotic program.* Cancer Res, 2000. **60**(20): p. 5673-80.
52. Salomon, D.S., et al., *The role of amphiregulin in breast cancer.* Breast Cancer Res Treat, 1995. **33**(2): p. 103-14.
53. Chen, Z., et al., *Hepatic SMARCA4 predicts HCC recurrence and promotes tumour cell proliferation by regulating SMAD6 expression.* Cell Death Dis, 2018. **9**(2): p. 59.
54. Guerrero-Martínez, J.A. and J.C. Reyes, *High expression of SMARCA4 or SMARCA2 is frequently associated with an opposite prognosis in cancer.* Sci Rep, 2018. **8**(1): p. 2043.
55. Banine, F., et al., *SWI/SNF chromatin-remodeling factors induce changes in DNA methylation to promote transcriptional activation.* Cancer Res, 2005. **65**(9): p. 3542-7.
56. Lakshman, M., et al., *CD44 promotes resistance to apoptosis in human colon cancer cells.* Exp Mol Pathol, 2004. **77**(1): p. 18-25.
57. Nam, K., et al., *CD44 regulates cell proliferation, migration, and invasion via modulation of c-Src transcription in human breast cancer cells.* Cell Signal, 2015. **27**(9): p. 1882-94.
58. Domínguez, G., et al., *Different expression of P14ARF defines two groups of breast carcinomas in terms of TP73 expression and TP53 mutational status.* Genes Chromosomes Cancer, 2001. **31**(2): p. 99-106.

59. Reijm, E.A., et al., *Decreased expression of EZH2 is associated with upregulation of ER and favorable outcome to tamoxifen in advanced breast cancer.* Breast Cancer Res Treat, 2011. **125**(2): p. 387-94.
60. Moelans, C.B., et al., *ESR1 amplification is rare in breast cancer and is associated with high grade and high proliferation: a multiplex ligation-dependent probe amplification study.* Cell Oncol (Dordr), 2011. **34**(5): p. 489-94.
61. Fujii, R., et al., *Increased androgen receptor activity and cell proliferation in aromatase inhibitor-resistant breast carcinoma.* J Steroid Biochem Mol Biol, 2014. **144 Pt B**: p. 513-22.
62. Singh, A.K., et al., *Advanced stage of breast cancer hoist alkaline phosphatase activity: risk factor for females in India.* 3 Biotech, 2013. **3**(6): p. 517-520.
63. den Hollander, P., et al., *Phosphatase PTP4A3 Promotes Triple-Negative Breast Cancer Growth and Predicts Poor Patient Survival.* Cancer Res, 2016. **76**(7): p. 1942-53.
64. Liu, T., et al., *The suppression of DUSP5 expression correlates with paclitaxel resistance and poor prognosis in basal-like breast cancer.* Int J Med Sci, 2018. **15**(7): p. 738-747.
65. Zakikhani, M., et al., *Metformin Is an AMP Kinase-Dependent Growth Inhibitor for Breast Cancer Cells.* Cancer Research, 2006. **66**(21): p. 10269-10273.
66. Alimova, I.N., et al., *Metformin inhibits breast cancer cell growth, colony formation and induces cell cycle arrest in vitro.* Cell Cycle, 2009. **8**(6): p. 909-915.
67. Liu, B., et al., *Metformin induces unique biological and molecular responses in triple negative breast cancer cells.* Cell Cycle, 2009. **8**(13): p. 2031-40.
68. Hirsch, H.A., et al., *Metformin selectively targets cancer stem cells, and acts together with chemotherapy to block tumor growth and prolong remission.* Cancer Res, 2009. **69**(19): p. 7507-11.
69. Oliveras-Ferraros, C., A. Vazquez-Martin, and J.A. Menendez, *Genome-wide inhibitory impact of the AMPK activator metformin on [kinesins, tubulins, histones, auroras and polo-like kinases] M-phase cell cycle genes in human breast cancer cells.* Cell Cycle, 2009. **8**(10): p. 1633-6.
70. Anisimov, V.N., et al., *Metformin decelerates aging and development of mammary tumors in HER-2/neu transgenic mice.* Bull Exp Biol Med, 2005. **139**(6): p. 721-3.
71. Kasznicki, J., A. Sliwinska, and J. Drzewoski, *Metformin in cancer prevention and therapy.* Ann Transl Med, 2014. **2**(6): p. 57.
72. Chae, Y.K., et al., *Repurposing metformin for cancer treatment: current clinical studies.* Oncotarget, 2016. **7**(26): p. 40767-40780.
73. Marrone, K.A., et al., *A Randomized Phase II Study of Metformin plus Paclitaxel/Carboplatin/Bevacizumab in Patients with Chemotherapy-Naïve Advanced or Metastatic Nonsquamous Non-Small Cell Lung Cancer.* Oncologist, 2018. **23**(7): p. 859-865.
74. Stauffer, S., et al., *KIBRA promotes prostate cancer cell proliferation and motility.* 2016: p. n/a-n/a.
75. Inoki, K., T. Zhu, and K.L. Guan, *TSC2 mediates cellular energy response to control cell growth and survival.* Cell, 2003. **115**(5): p. 577-90.
76. Beronja, S., et al., *Rapid functional dissection of genetic networks via tissue-specific transduction and RNAi in mouse embryos.* Nat Med, 2010. **16**(7): p. 821-7.

77. Xiao, L., et al., *KIBRA Regulates Hippo Signaling Activity via Interactions with Large Tumor Suppressor Kinases.* Journal of Biological Chemistry, 2011. **286**(10): p. 7788-7796.
78. Sakuma, T., et al., *Multiplex genome engineering in human cells using all-in-one CRISPR/Cas9 vector system.* Scientific Reports, 2014. **4**(1).
79. Zhou, J., et al., *Zyxin promotes colon cancer tumorigenesis in a mitotic phosphorylation-dependent manner and through CDK8-mediated YAP activation.* Proc Natl Acad Sci U S A, 2018. **115**(29): p. E6760-E6769.
80. Zeng, Y., et al., *Cyclin-dependent kinase 1 (CDK1)-mediated mitotic phosphorylation of the transcriptional co-repressor Vgll4 inhibits its tumor-suppressing activity.* J Biol Chem, 2017. **292**(36): p. 15028-15038.
81. Chen, X., et al., *Ajuba Phosphorylation by CDK1 Promotes Cell Proliferation and Tumorigenesis.* J Biol Chem, 2016. **291**(28): p. 14761-72.
82. Dobin, A., et al., *STAR: ultrafast universal RNA-seq aligner.* Bioinformatics, 2012. **29**(1): p. 15-21.
83. Li, B. and C.N. Dewey, *RSEM: accurate transcript quantification from RNA-Seq data with or without a reference genome.* BMC Bioinformatics, 2011. **12**(1): p. 323.
84. Benjamini, Y. and Y. Hochberg, *Controlling the False Discovery Rate: A Practical and Powerful Approach to Multiple Testing.* Journal of the Royal Statistical Society. Series B (Methodological), 1995. **57**(1): p. 289-300.

Figures

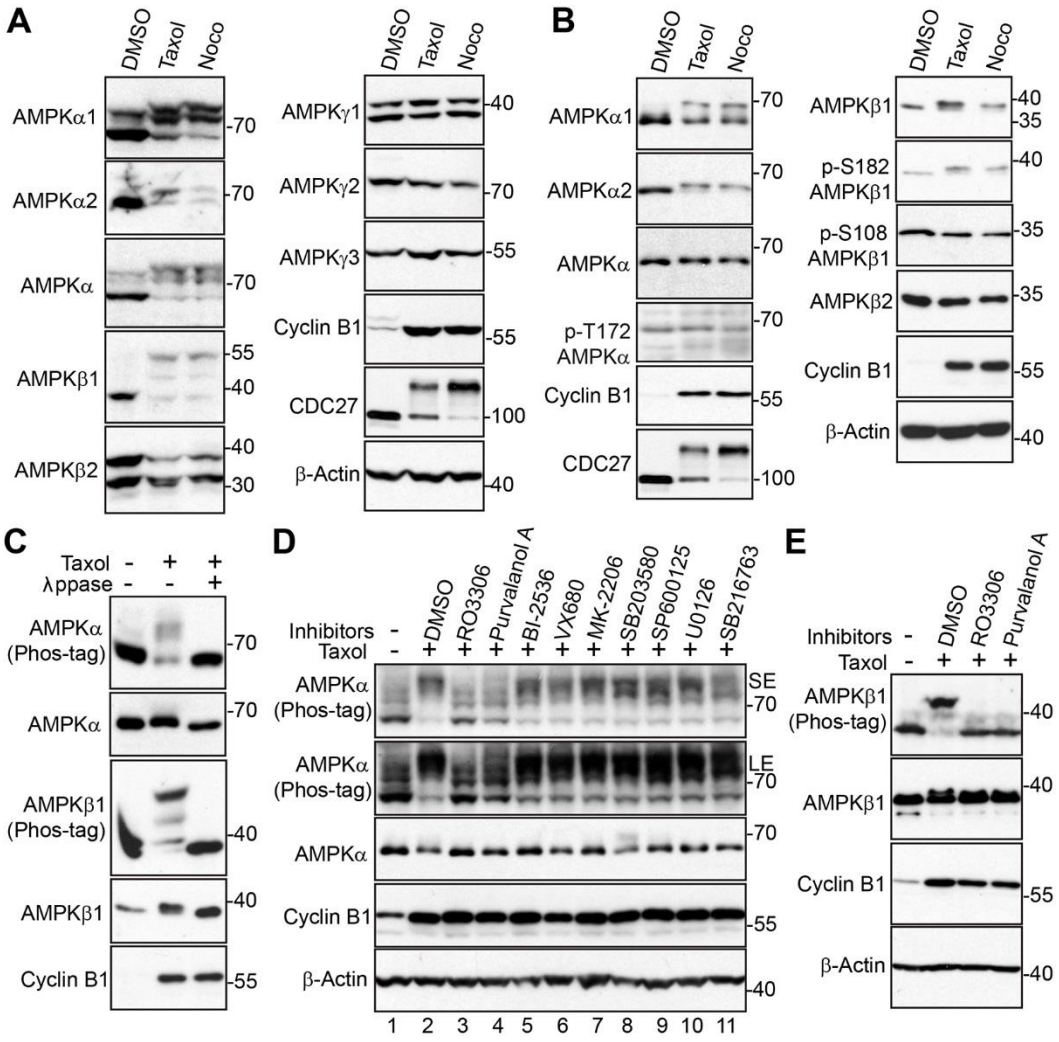

Figure 1. Phosphorylation of AMPK subunits by CDK1 during mitotic arrest.

A, HeLa cells were treated with DMSO, taxol (100 nM for 16 h) or nocodazole (100 ng/mL for 16 h). Total cell lysates were probed on Phos-tag™ SDS polyacrylamide gels with the indicated antibodies. Cyclin B1, CDC27, and β-Actin blots were from regular gels.

B, Total cell lysates from A were electrophoresed on regular SDS polyacrylamide gels and probed with the indicated antibodies.

C, HeLa cells were treated with taxol as indicated and cell lysates were further treated with (+) or without (−) λ-phosphatase (ppase). Total cell lysates were probed with the indicated antibodies.

D, HeLa cells were treated with taxol, with or without various kinase inhibitors as indicated. RO3306 (5 μM), Purvalanol A (10 μM), BI-2536 (100 nM), VX680 (2 μM), MK-2206 (10 μM), SB203580 (10 μM), SP600125 (20 μM), U0126 (20 μM), and SB216763 (10 μM) were used. Inhibitors were added 1 h before harvesting the cells (with MG132 to prevent Cyclin B degradation and subsequent mitotic exit). Total cell lysates were electrophoresed on regular and Phos-tag™ SDS polyacrylamide gels and probed with the indicated antibodies.

E, HeLa cells were treated with taxol, with or without the CDK1 inhibitors as indicated. RO3306 (5 μM), Purvalanol A (10 μM). Total cell lysates were electrophoresed on regular and Phos-tag™ SDS polyacrylamide gels and probed with the indicated antibodies.

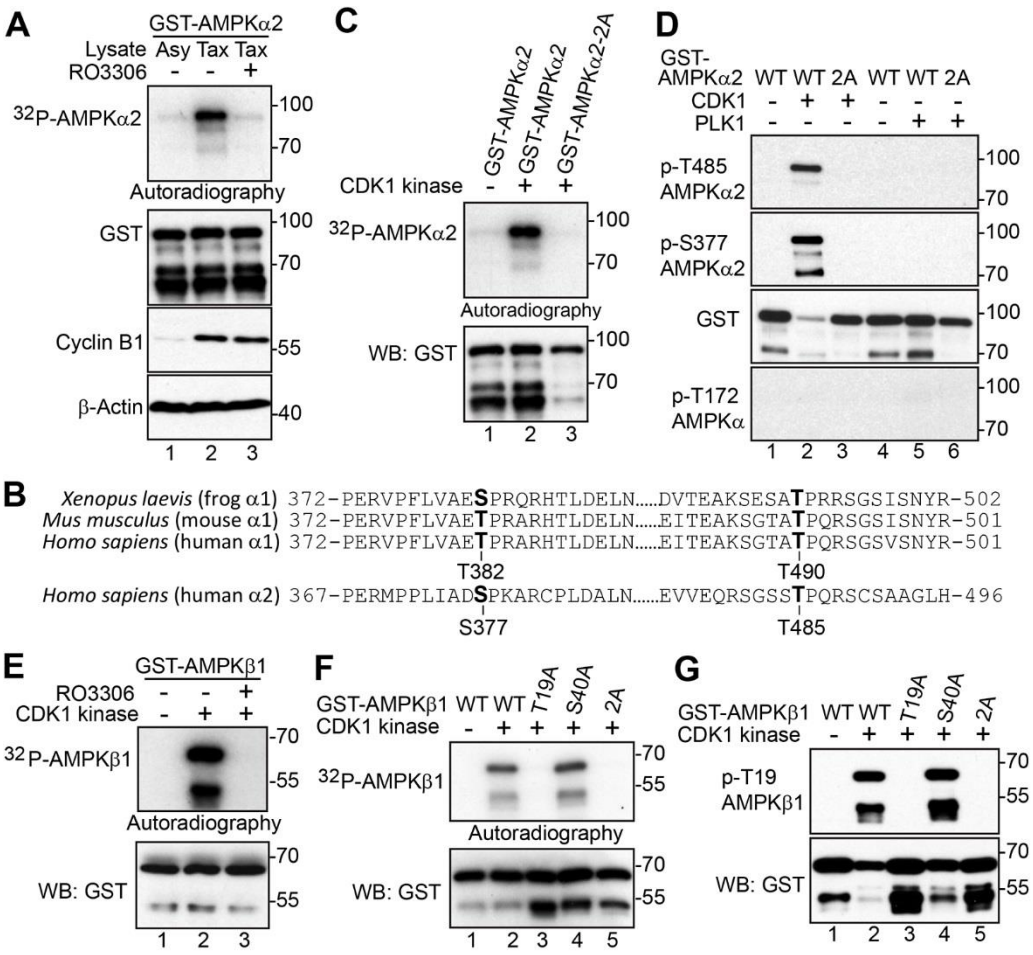

Figure 2. CDK1 phosphorylates AMPK subunits *in vitro*.

A, *In vitro* ^{32}P kinase assays with lysates of mitotically arrested cells and recombinant GST-AMPKα2. RO3306 (5 μM) was used to inhibit CDK1 kinase activity.

B, Conservation of AMPK's mitotic phosphorylation sites.

C, *In vitro* ^{32}P kinase assays with purified CDK1/Cyclin B1 complex and recombinant GST-AMPKα2 or GST-AMPKα2-2A (S377A/T485A).

D, *In vitro* kinase assays with purified CDK1/Cyclin B1 complex or activated PLK1 and recombinant GST-AMPKα2 or GST-AMPKα2-2A and probed with phospho-antibodies.

E, *In vitro* ^{32}P kinase assays with purified CDK1/Cyclin B1 complex and recombinant GST-AMPKβ1. RO3306 (5 μM) was used to inhibit CDK1 kinase activity.

F, *In vitro* ^{32}P kinase assays with purified CDK1/Cyclin B1 complex to phosphorylate recombinant GST-AMPKβ1, GST-AMPKβ1-T19A, GST-AMPKβ1-S40A, or GST-AMPKβ1-2A. G, In vitro kinase assays using purified CDK1/Cyclin B1 complex to phosphorylate recombinant GST-AMPKβ1, GST-AMPKβ1-T19A, GST-AMPKβ1-S40A, or GST-AMPKβ1-2A (T19A/S40A) and probed with phospho-antibody.

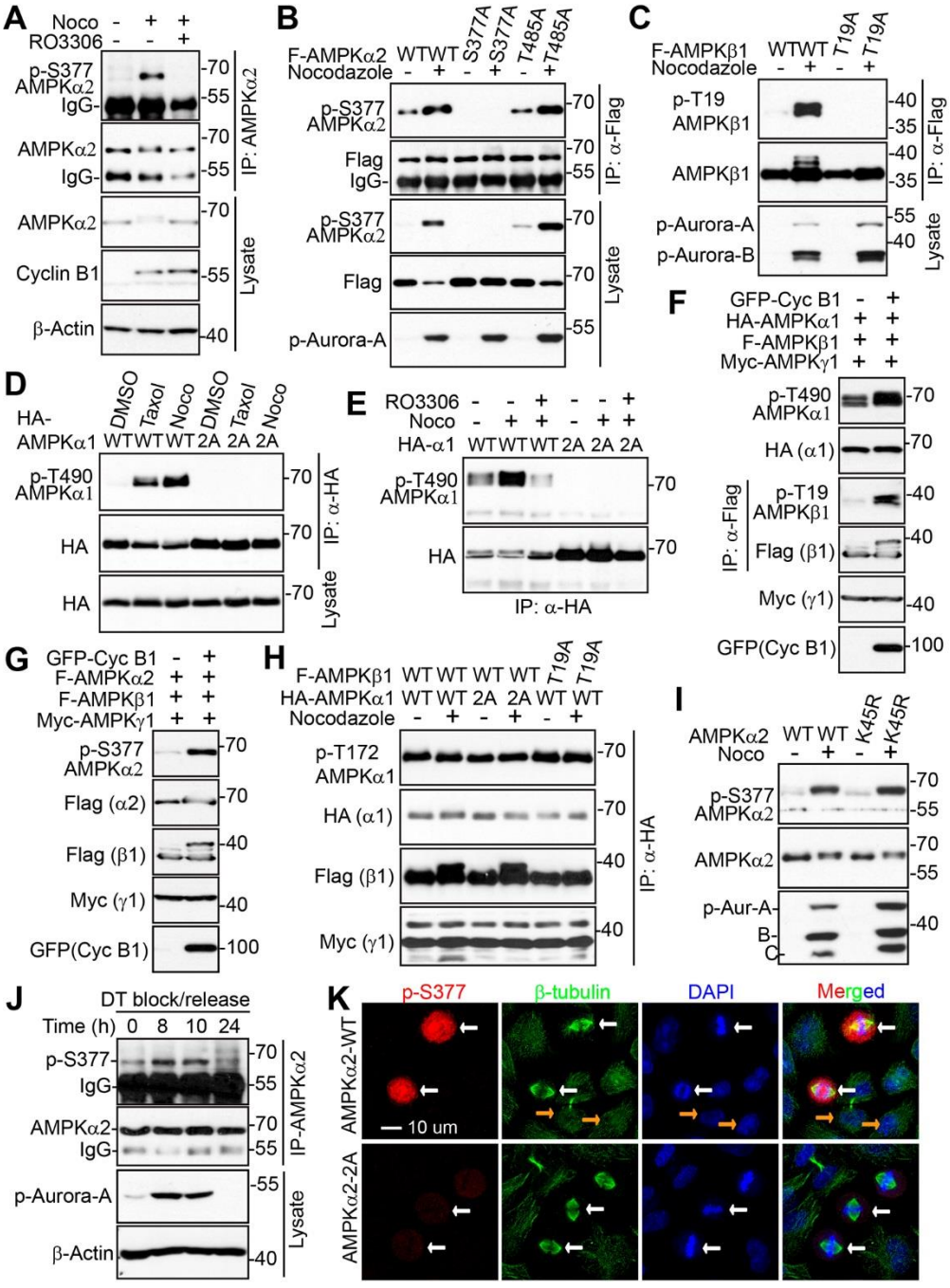

Figure 3. CDK1 phosphorylates AMPK subunits in cells.

A, Endogenous AMPKα2 immunoprecipitation in HeLa cells treated with nocodazole (16 h) or nocodazole (16 h) with RO3306 and MG132 (1 h) and probed with p-S377 antibody.

B, HEK293T cells transfected with Flag-AMPKα2-WT, Flag-AMPKα2-S377A, or Flag-AMPKα2-T485A and treated with taxol or nocodazole (16 h). Flag-tagged proteins were immunoprecipitated, then probed with p-S377 antibody.

C, HEK293T cells were transfected with Flag-AMPKβ1-WT or Flag-AMPKβ1-T19A and treated with taxol or nocodazole (16 h). Flag-tagged proteins were immunoprecipitated, then probed with p-T19 antibody.

D, HEK293T cells transfected with HA-AMPKα1-WT or HA-AMPKα1-2A (T382A/T490A) and treated with taxol or nocodazole (16 h). HA-tagged proteins were immunoprecipitated, then probed with p-T490 antibody.

E, HEK293T cells transfected with HA-AMPKα1-WT or HA-AMPKα1-2A and treated with nocodazole (16 h) or nocodazole (16 h) with RO3306 and MG132 (1 h). HA-tagged proteins were immunoprecipitated, then probed with p-T490 antibody.

F, G, HEK293T cells were transfected as indicated. At 48 h post-transfection, immunoprecipitated samples or total cell lysates were subjected to Western blotting with the indicated antibodies. GFP-Cyclin B1 is a constitutive active form of GFP-tagged Cyclin B1 (R42A non-degradable mutant).

H, Co-immunoprecipitation of HA-tagged protein in HEK293T cells co-transfected with Myc-AMPKγ1, either HA-AMPKα1-WT or HA-AMPKα1-2A, and Flag-AMPKβ1-WT or Flag-AMPKβ1-T19A in HEK293T cells treated with nocodazole, then probed with the indicated antibodies.

I, Total lysates of HEK293T cells transfected with Flag-AMPKα2-WT or Flag-AMPKα2-K45R and treated with nocodazole, probed with p-S377.

J, HeLa cells were synchronized by a double thymidine (DT) block and release method and collected at the indicated time points. AMPKα2 proteins were immunoprecipitated and subjected to Western blotting with the indicated antibodies. Increased p-Aurora A levels mark cells in mitosis.

K, Immunofluorescence staining of p-S377 AMPKα2 in freely cycling HeLa cells stably expressing AMPKα2-WT or AMPKα2-2A (S377A/T485A). White arrows mark cells in metaphase or anaphase (condensed and aligned chromosomes). Yellow arrows mark cells in interphase or cytokinesis.

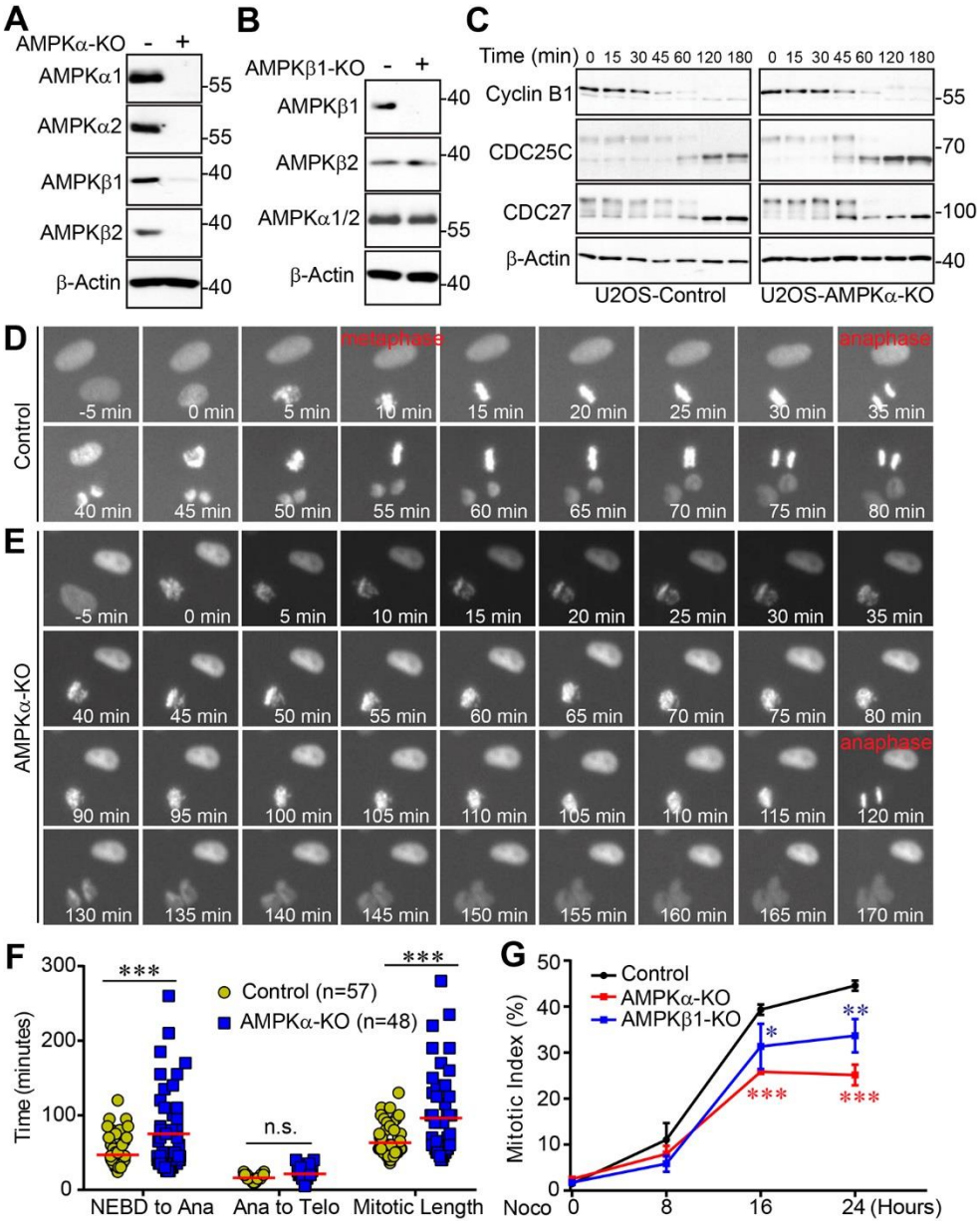

Figure 4. AMPK is required for normal mitotic entry and progression.

A, B, Western blots of U2OS, U2OS AMPK β1-KO, and U2OS AMPKα-KO (AMPKα1/α2 double KO) cells probed for various AMPK subunits.

C, HeLa cells arrested in mitosis with nocodazole (16 h) which were subsequently washed and released into fresh medium for collection at the specified time points and then probed with the indicated antibodies.

D, E, Live-cell imaging of RFP-H2B expressing U2OS or U2OS AMPKα-KO cells entering and exiting mitosis.

F, Quantification of mitotic phase timing from live-cell data. ***: $p<0.001$ (Two-way ANOVA). N.S.: not significant.

G, Mitotic index time-course measurements of U2OS, U2OS AMPK β1-KO, and U2OS AMPKα-KO treated with nocodazole. Data were expressed as mean ± SEM from three independent experiments. *: $p<0.05$, **: $p<0.01$, ***: $p<0.001$ (t-test).

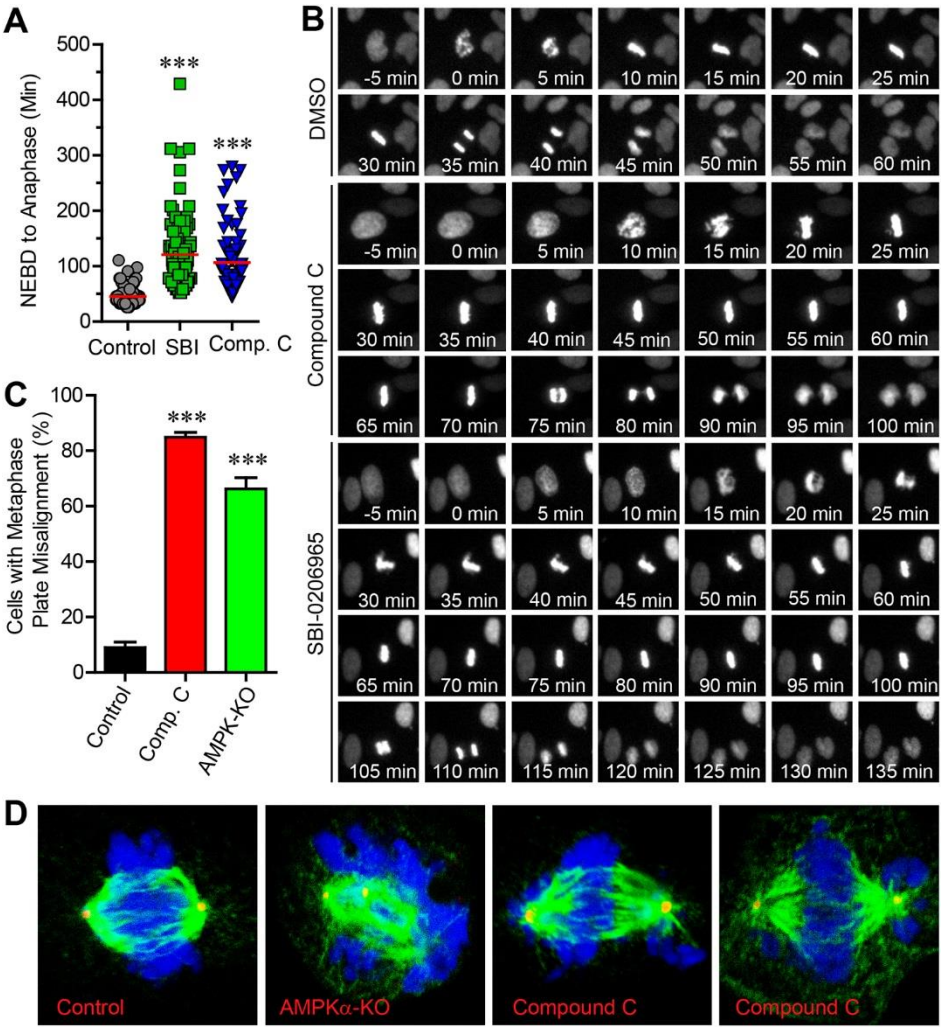

Figure 5. Small-molecule inhibition of AMPK kinase activity phenocopies AMPKα-KO.

A, Live-cell image quantification of nuclear envelope breakdown (NEBD) to anaphase length in RFP-H2B-expressing U2OS cells treated with 5 μM SBI-0206965 (SBI) or 5 μM Compound C (Comp C) for 24h. ***: $p<0.001$ (t-test). 100 cells were analyzed for each group in 4 separate experiments.

B, Representative live-cell images demonstrating mitotic length of cells quantified in (A).

C, Confocal microscopy of fixed AMPKα-KO U2OS or U2OS cells treated with Comp C were used for quantification of abnormal metaphase plate alignment. ***: $p<0.001$ (t-test). Total cells analyzed: Control=102, Comp. C=103, AMPKα-KO=122 in 4 separate experiments.

D, Representative confocal images of cells analyzed in (C). DAPI is blue, α-tubulin is green, and γ-tubulin is red.

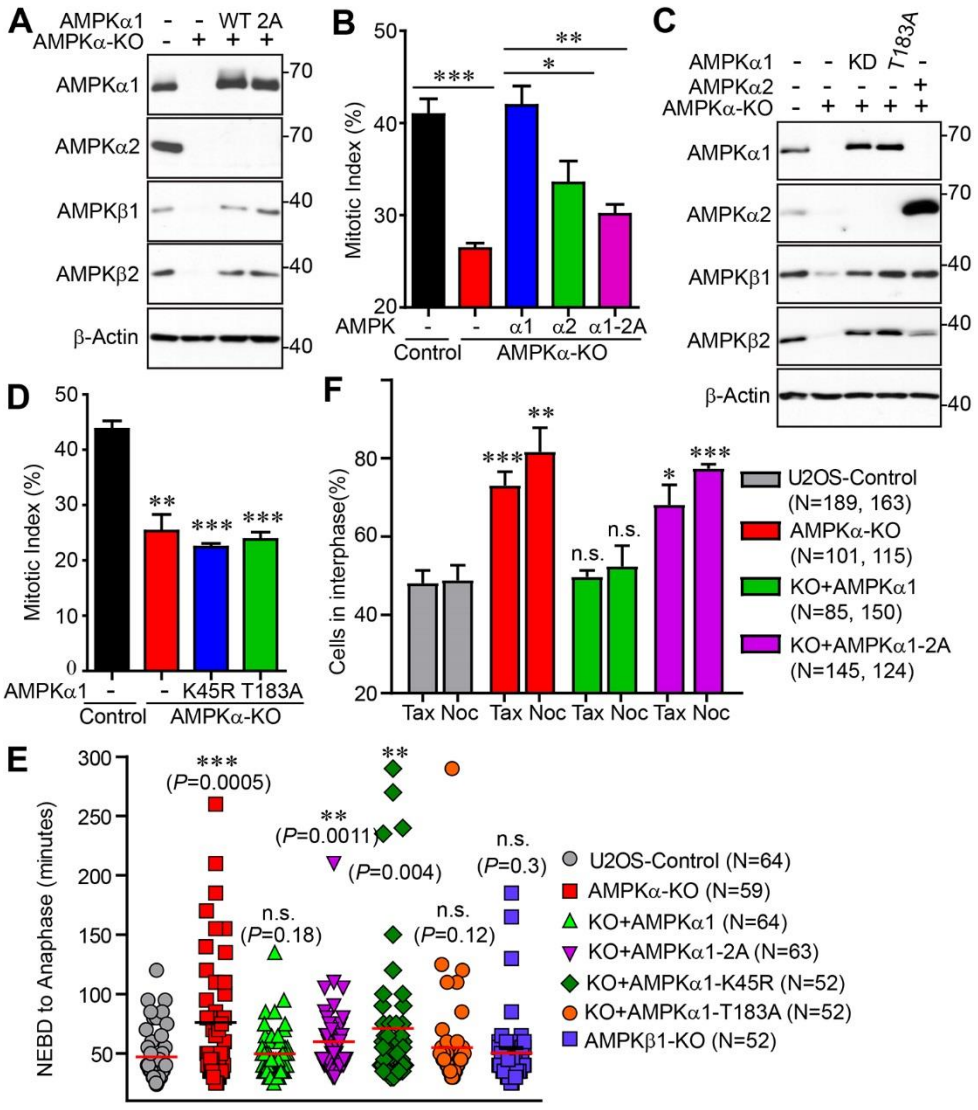

Figure 6. AMPKα1 re-expression can rescue AMPKα-KO mitotic phenotypes.

A, Western blots of U2OS AMPKα-KO cells stably expressing AMPKα1-WT or AMPKα1-2A, probed for various AMPK subunits.

B, Mitotic index of cells treated with nocodazole (16 h). Data were expressed as mean ± SEM from three independent experiments. *: p<0.05, **: p<0.01, ***: p<0.001 (t-test).

C, Western blots of U2OS AMPKα-KO cells stably expressing AMPKα1-K45R, AMPKα1-T183A, or AMPKα2-WT, probed for various AMPK subunits.

D, Mitotic index of cells treated with nocodazole (16 h). Data were expressed as mean ± SEM from three independent experiments. **: p<0.01, ***: p<0.001 (t-test).

E, Quantification of mitotic phase timing from live-cell imaging of RFP-H2B-expressing cells entering and exiting mitosis for 24 h. **: p<0.01, ***: p<0.001 (Mann Whitney U-test). U2OS n=64, AMPKα-KO n=59, α1-WT n=64, α1-2A n=63, α1-K45R n=52, α1-T183A n=52, AMPKβ1-KO n=52. N.s.: not significant.

F, Quantification of live-cell imaging of the percentage of cells remaining in interphase when treated with nocodazole for 24 h. *: p<0.05, **: p<0.01, ***: p<0.001 (t-test). Total cells analyzed: U2OS Taxol=189, U2OS Nocodazole=163, AMPKα-KO Taxol=101, AMPKα-KO Nocodazole=115, α1-WT Taxol=85, α1-WT Nocodazole=150, α1-2A Taxol=145, and α1-2A Nocodazole=124 in 4 separate experiments. N.s.: not significant.

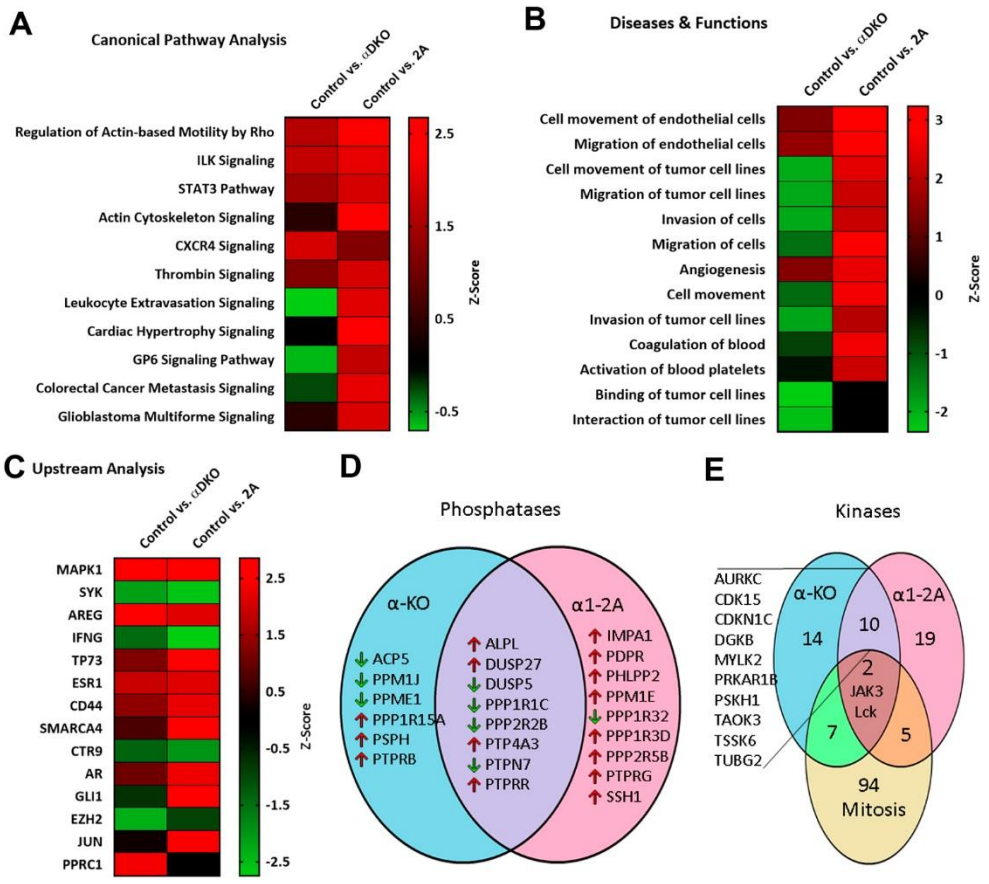

Figure 7. RNA-Seq analysis of AMPKα-KO and AMPKα1-2A U2OS cells.

A, Top canonical pathways altered in AMPKα-KO and AMPKα-KO reconstituted with AMPKα1-2A U2OS cells derived from ingenuity pathway analysis (IPA) gene ontology algorithms.

B, Top diseases and biological functions found enriched in AMPKα-KO and α1-2A reconstituted U2OS cells.

C, Upstream regulators predicted to be activated or inhibited based on genes that were significantly different for parental U2OS and AMPKα-KO or α1-2A reconstituted U2OS cells.

D, Comparison of phosphatases more than 2-fold altered in AMPKα-KO and α1-2A reconstituted U2OS cells.

E, Kinases identified by IPA gene ontology algorithms as mitotic kinases compared with kinases more than 2-fold altered in AMPKα-KO and α1-2A reconstituted U2OS cells.

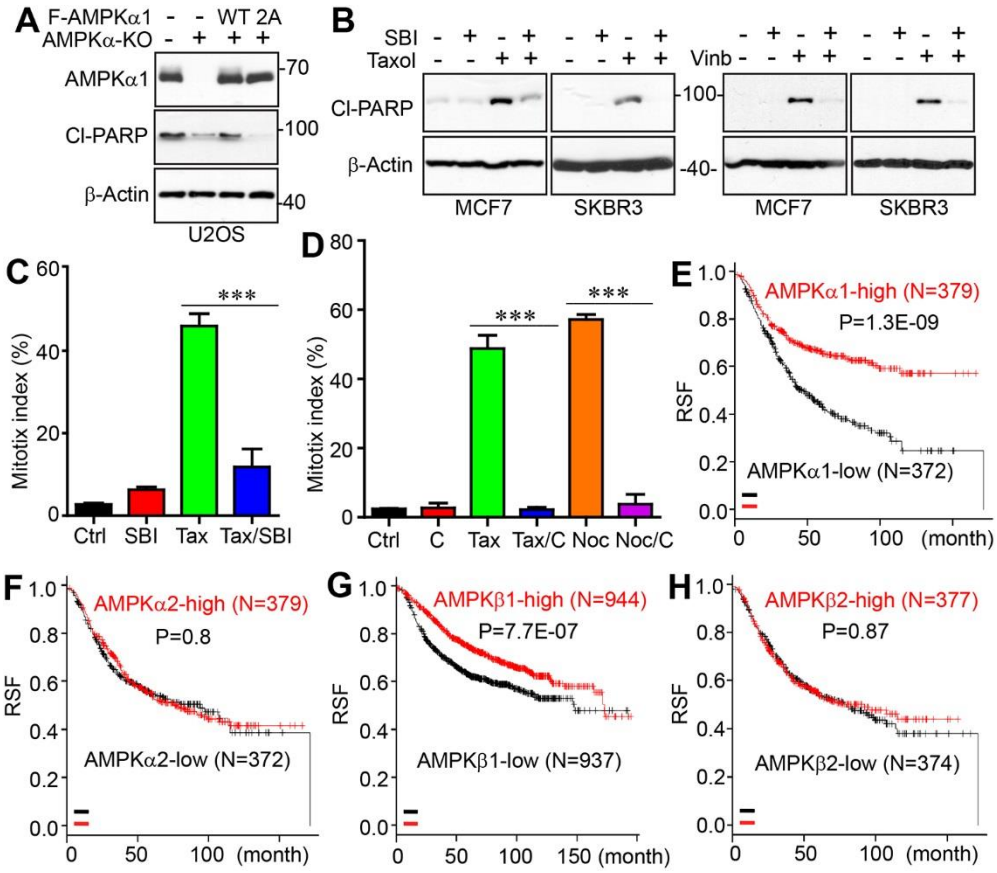

Figure 8. AMPK expression and kinase activity are crucial for paclitaxel drug sensitivity and breast cancer patient relapse-free survival.

A, Western blot of U2OS, AMPKα-KO, AMPKα1-WT and AMPKα1-2A cells treated with taxol (100 nM) for 24 h and probed for cleaved PARP.

B, Western blot of MCF7 and SKBR3 cells treated with SBI (1 μM) and taxol (500 nM and 100 nM respectively) for 24 h and probed for cleaved PARP. SBI: SBI-0206965. Vinb: vinblastine.

C, Mitotic indexes of HeLa cells treated with taxol alone, SBI alone, or taxol with SBI.

D, Mitotic indexes of HeLa cells treated with taxol alone, nocodazole alone, Compound C alone, taxol with Compound C, or nocodazole with Compound C. Data (C, D) were expressed as mean ± SEM from three independent experiments. ***: $p<0.001$ (t-test).

E-H, Kaplan-Meier curves of relapse-free survival vs. PRKAA1 (E), PRKAA2 (F), PRKAB1 (G), and PRKAB2 (H) expression in breast cancer patients treated systemically. Data were generated from an online survival analysis tool, KM Plotter, using microarray data of 1,809 patients [47].

Table S1

AMPK guide sequences

Oligo name	Sequence
PRKAB1-A-Fwd	caccGCAGCGCGGCGCGCTCACTGC
PRKAB1-A-Rev	aaacGCAGTGAGCGCGCCGCGCTGC
PRKAB1-B-Fwd	caccGTGGCCATAAGACGCCCCGG
PRKAB1-B-Rev	aaacCCGGGGCGTCTTATGGCCAC
PRKAA1-A-Fwd	caccGGCTGTCGCCATCTTTCTCC
PRKAA1-A-Rev	aaacGGAGAAAGATGGCGACAGCC
PRKAA1-B-Fwd	caccGAAGATCGGCCACTACATTC
PRKAA1-B-Rev	aaacGAATGTAGTGGCCGATCTTC
PRKAA2-A-Fwd	caccGTCAGCCATCTTCGGCGCGCG
PRKAA2-A-Rev	aaacCGCGCGCCGAAGATGGCTGAC
PRKAA2-B-Fwd	caccGAAGATCGGACACTACGTGC
PRKAA2-B-Rev	aaacGCACGTAGTGTCCGATCTTC

Fwd: forward; Rev: reverse

Supplemental Figure 1

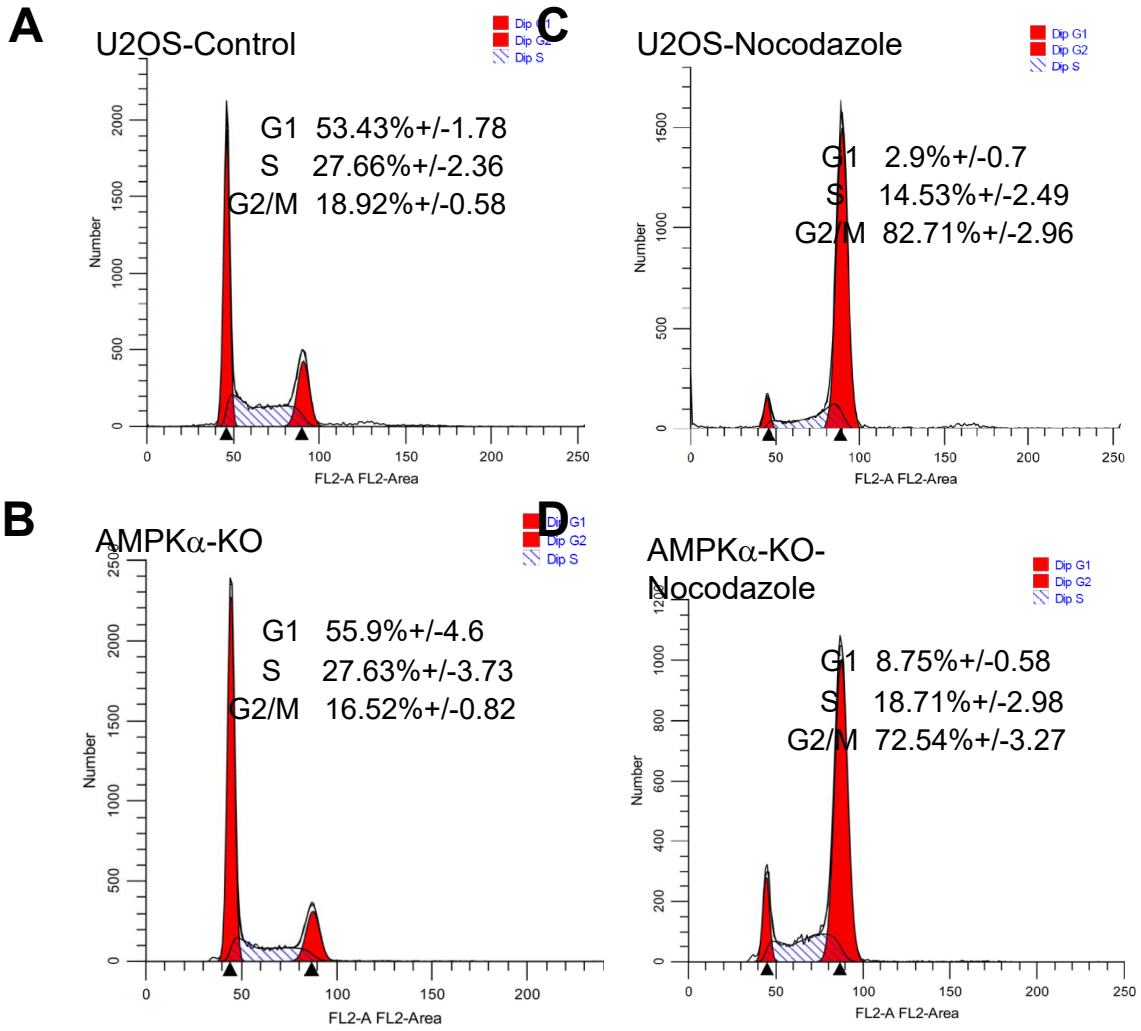

Fig. S1 FACS analysis of control and AMPKα-KO cells. Cells were treated with DMSO (control) (**A, B**) or Nocodazole (100 ng/mL for 20 h) (**C, D**) and cells were then stained by PI analyzed by flow cytometry. Numbers for each cell cycle phases are from three repeats.

Table S1

AMPK guide sequences

Oligo name	Sequence
PRKAB1-A-Fwd	caccGCAGCGCGGCGCGCTCACTGC
PRKAB1-A-Rev	aaacGCAGTGAGCGCGCCGCGCTGC
PRKAB1-B-Fwd	caccGTGGCCATAAGACGCCCCGG
PRKAB1-B-Rev	aaacCCGGGGCGTCTTATGGCCAC
PRKAA1-A-Fwd	caccGGCTGTCGCCATCTTTCTCC
PRKAA1-A-Rev	aaacGGAGAAAGATGGCGACAGCC
PRKAA1-B-Fwd	caccGAAGATCGGCCACTACATTC
PRKAA1-B-Rev	aaacGAATGTAGTGGCCGATCTTC
PRKAA2-A-Fwd	caccGTCAGCCATCTTCGGCGCGCG
PRKAA2-A-Rev	aaacCGCGCGCCGAAGATGGCTGAC
PRKAA2-B-Fwd	caccGAAGATCGGACACTACGTGC
PRKAA2-B-Rev	aaacGCACGTAGTGTCCGATCTTC

Fwd: forward; Rev: reverse

Supplemental Figure 1

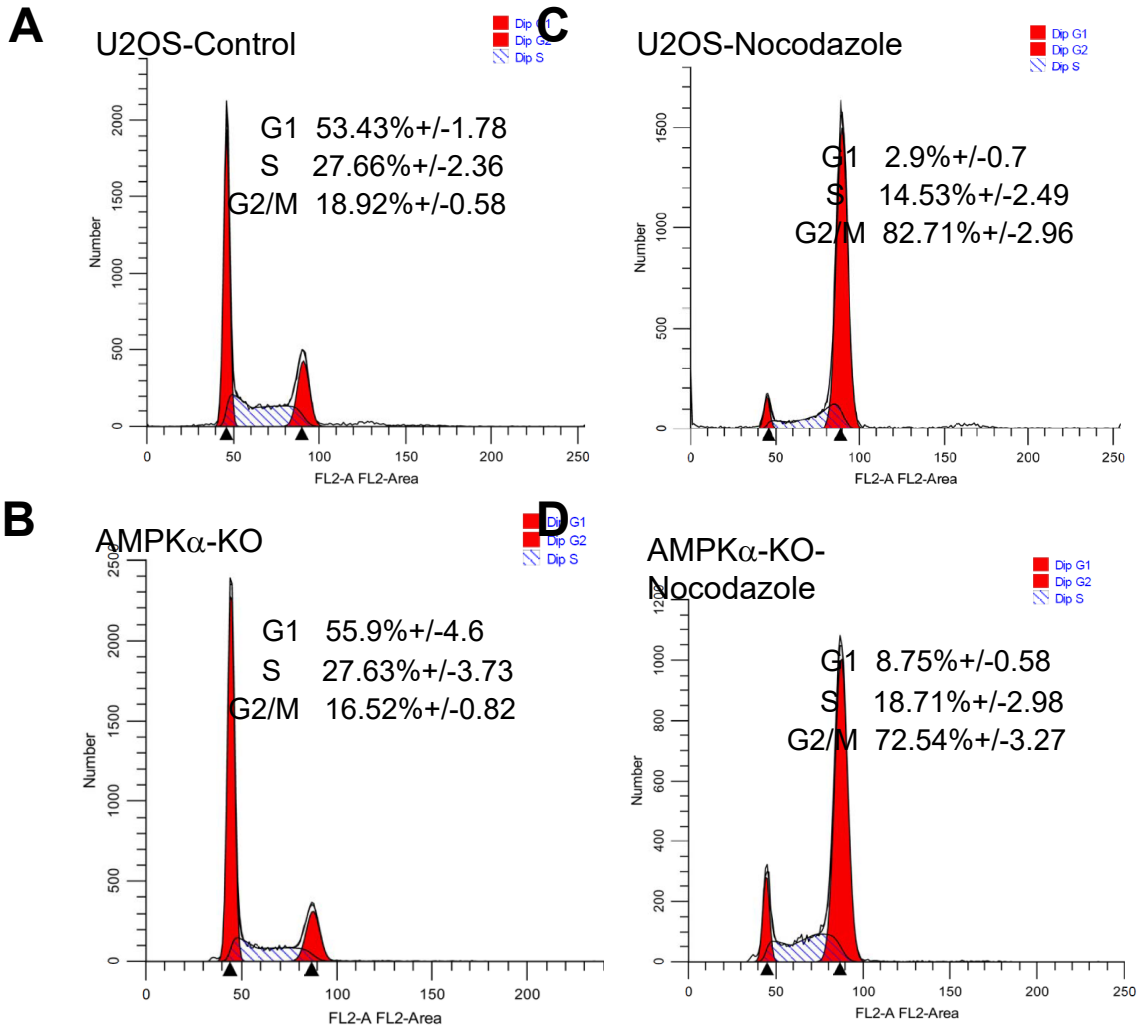

Fig. S1 FACS analysis of control and AMPKα-KO cells. Cells were treated with DMSO (control) (**A, B**) or Nocodazole (100 ng/mL for 20 h) (**C, D**) and cells were then stained by PI analyzed by flow cytometry. Numbers for each cell cycle phases are from three repeats.